THESIS

UPLAND PROCESSES AND CONTROLS ON SEPTEMBER 2013 DEBRIS FLOWS, ROCKY MOUNTAIN NATIONAL PARK, COLORADO

Submitted by

Annette Patton

Department of Geosciences

In partial fulfillment of the requirements

For the Degree of Master of Science

Colorado State University

Fort Collins, Colorado

Summer 2016

Master's Committee:

Advisor: Sara Rathburn

Ellen Wohl
Jeffrey Niemann
Eric Bilderback

ABSTRACT

UPLAND PROCESSES AND CONTOLS ON SEPTEMBER 2013 DEBRIS FLOWS, ROCKY MOUNTAIN NATIONAL PARK, COLORADO

More than 10 large debris flows occurred in and near Rocky Mountain National Park (RMNP) following the spatially extensive September 2013 rainstorm in the Colorado Front Range. These debris flows delivered sediment to valley bottoms and had the potential to damage infrastructure and endanger park visitors and staff. To characterize conditions of debris flow initiation when known thresholds of elevation, slope angle, and rainfall intensity are met, 11 debris flow sites in RMNP were surveyed. Slope variables including soil depth, soil texture, and slope morphology were compared between 11 failed and 30 undisturbed hillslopes (control sites) that were exposed to similar cumulative rainfall during the 2013 storm.

Analysis of measured slope variables indicates that slope morphology is strongly related to debris flow occurrence. Four of the 11 surveyed debris flows initiated in or immediately below a colluvial hollow (a topographic concavity on a hillslope), while only 1/30 control sites were located near a colluvial hollow. Furthermore, 8/11 surveyed debris flows initiated in areas of convergent topography (including colluvial hollows and areas of broader convergence), while only 3/30 control slopes were convergent. The differences in these proportions suggest that hillslopes characterized by a colluvial hollow or other convergent topography accumulate surface and groundwater flow and collect unconsolidated material. Convergent hillslopes are therefore more susceptible to slope failure during rain events of sufficient intensity and/or duration. The other geomorphic hillslope variables evaluated in this study did not demonstrate statistically

significant differences between debris flow sites and control sites. In some cases, small sample size or other data constraints may provide limited ability to discern geomorphic differences between debris flows and control sites.

The Bighorn site, a large debris flow near an historic structure in RMNP, was selected for detailed geochronologic study to determine the ages of old debris deposits and evaluate debris flow frequency. Several numeric and relative dating techniques were applied to determine the age of pre-2013 debris deposits at this site. Numeric dating techniques included radiocarbon analysis of organic material and ^{10}Be radionuclide analysis of boulders collected from four debris flow levees. ^{10}Be exposure dating has not previously been applied to debris flow surfaces.

Mapping of debris flow levees and stratigraphic study at the Bighorn debris flow site confirm that at least 2-3 and possibly more debris flows have occurred at this site within the last 10^2-10^3 years. The recurrence of debris flows at this site indicates that it may experience similar mass movements in the future. A boulder sample collected from the 2013 debris flow levee returned an 18.1 ka ^{10}Be exposure age. Ranges of exposure ages for three older debris deposits are 54.2, 143, and 121 ka. The falsely old age of the 2013 sample and the wide range of ages determined for each of the older landforms indicate that exposure histories of debris deposits are complicated by inherited atmospheric exposure prior to debris flows. Radiocarbon ages of material collected from this site are on the order of 10^0-10^2 years old and do not cluster according to the landform sampled.

The results of this study demonstrate that debris flow initiation is governed by a complex interaction of geomorphic and climate variables across a range of spatial and temporal scales. Additionally, the scatter of ages established for old debris flow deposits at the Bighorn debris flow site suggests that debris deposits continue to be modified by secondary processes after the initial event. The downslope pathway of debris flow material reflects highly individual histories from source to sink to deposition near the valley bottom. The numerous debris flows that initiated in the 2013 storm exemplify ongoing debris flow hazards in the Colorado Front Range and highlight the need for awareness of hillslope hazards in this region.

ACKNOWLEDGEMENTS

I would like to express my sincere gratitude to the many people and organizations who made this research possible. First and foremost, thank you to my advisor, Dr. Sara Rathburn, whose support, academic guidance, and personal advice were fundamental to the completion of this project. I have enjoyed working with such a conscientious and welcoming mentor, and look forward to continuing to learn from your experience in the upcoming years. Thank you also to Dr. Eric Bilderback for his unfailing willingness to share his geomorphic expertise, encouragement, and field-ready hiking legs. Deepest thanks to Dr. Jeff Niemann and Dr. Ellen Wohl for sharing their time and advice on my thesis committee. Sincere thanks also to Paul McLaughlin and Scott Esser for logistic support; to Nick Santiago, Garth Hesseltine, Dave Dust, Derek Schook, and Dan Scott for field help; to Claire Lukens for her generous donation of time and knowledge in collecting, processing, and analyzing ^{10}Be data; to Tom Clifton and the Purdue PRIME lab for assistance processing and analyzing ^{10}Be samples. I would also like to thank Ann Hess and the Colorado State University statistics lab for statistical consultations. I must also declare my sincerest gratitude to my OTF, Krista Garrett, for research advice, camaraderie, and emotional support. I will sincerely miss sharing all of my best and worst experiences with you. Lastly, thank you to my parents, Kent and Julie Weiss, and my sister, Rebecca Wolfe. You have given me your unfailing support in all of my endeavors, from learning to ride a bike to embarking on one academic adventure after another. Thank you for teaching me the confidence to tackle even the steepest of debris flows. Thank you also to Rocky Mountain National Park, the National Park Service, the American Water Resources Association, the Colorado Scientific Society, the Rocky Mountain Association of Geologists, the Association of Environmental and Engineering Geologists, and Colorado State University for funding this project.

TABLE OF CONTENTS

1. INTRODUCTION

1.1 Introduction to debris flows

In mountainous regions, abrupt mass movements of hillslope sediment occur frequently and are important in shaping high-relief landscapes (Schuster and Highland, 2007). Mass movements are capable of disturbing large areas, destroying vegetation, and delivering large pulses of sediment to upland streams (Stock and Dietrich, 2006; Schuster and Highland, 2007; Goode et al., 2012). Debris flows are estimated to perform the majority of sediment transport in high-relief areas of the Colorado Front Range, influencing long-term erosion and exhumation rates of the Southern Rocky Mountains (Anderson et al., 2015).

Debris flows are a type of rapid mass movement characterized by a ratio of water to sediment that is intermediate between that of landslides and water floods (Costa and Jarrett, 1981). As such, the term "debris flow" is often used to include a number of mass movement events in which solids and liquids interact, including debris slides, debris torrents, debris floods, mudflows, hyper-concentrated flows, and lahars (Iverson, 1997). Thresholds of sediment concentration and their influence on fluid rheology distinguish debris flows from other sediment-rich flows including hyper-concentrated flows and sediment-laden water floods (Pierson, 2005). According to commonly used definitions, the volumetric sediment concentration of debris flows exceeds 40 percent and allows for fluidized movement of large volumes of hillslope material (Iverson, 2014). Debris flows of moderate size (approximately 10^3 m^3) are therefore simultaneously capable of traveling long distances and denuding vegetation, clogging drainage networks, damaging structures, and endangering humans (Iverson, 1997).

1.1.1 Debris flow mechanics

Debris flows initiate from disturbance by surface or groundwater, including coalescing rills, shallow landslides, or concentration of overland flow in bedrock channels (Godt and Coe, 2007). Most debris flows in the regions with temperate climates initiate as shallow landslides (Guthrie et al., 2010). Slope failure is possible when marginally stable debris is partly to fully saturated by a rapid increase in groundwater, usually from high-intensity rainfall or snowmelt (Costa, 1984; Iverson, 2014). Saturated debris fails when the internal pore pressure becomes sufficient to overcome the resisting frictional and cohesive forces of the hillslope material and loose debris begins to shear (Iverson, 1997). As saturated debris begins to move downslope, contraction of the material increases pore pressure and causes liquefaction, which results in internal deformation that is recognizable as flow (Iverson, 2014).

Once saturated debris begins moving downslope, debris flows appear to flow like wet concrete and can transport very large boulders in the dense fluid (Iverson, 1997, 2014). Once in motion, large debris flows can achieve speeds greater than 10 m/s (Iverson, 1997, 2014). Steep surge fronts form the head of the debris flow and contain disproportionately large concentrations of boulders, logs, and other objects relative to the main body of the flow (Iverson, 1997, 2014). More fluidized, finer-grained debris follows the dense fronts, impounded behind the dam-like surge front (Iverson, 2014). Highly fluidized water flows or hyper-concentrated flows may trail debris flows and rework debris deposits (Costa, 1984). Where increased friction dissipates energy along the front and lateral margins of the flow, elevated levees concentrate coarse debris and other large particles, often resulting in levee deposits that parallel the flow direction (Iverson, 1997).

Erosion by debris flows can scour channels in unconsolidated material and/or bedrock, particularly in the steepest portions of the flow path near the initiation site (Stock and Dietrich, 2006). Because of their erosive power, debris flow volume increases downslope of the initiation site as the flow entrains additional water, sediment, and organic material (Stock and Dietrich, 2006; Iverson et al., 2010; Iverson, 2014; Frank et al., 2015). Debris flows that travel across forested slopes commonly entrain large pieces of wood (Iverson, 2014).

Unlike deposits delivered by water floods, debris deposits are characteristically poorly sorted (Costa, 1984; Iverson, 1997; Pierson, 2005; Iverson, 2014). Debris deposits can include both lateral levees along the margins of the flow and fanlike lobes of sediment where frictional forces at the flow-front are sufficient to halt the flow (Costa, 1984; Iverson, 1997, 2014). Debris fans are typically deposited where steep hillslopes meet shallower valley floors (Costa, 1984; Iverson, 1997) as the effect of gravitational forces is reduced on low-angle slopes. Through time, hillslopes that source multiple debris flows can build extensive sediment fans that contain varying proportions of alluvial and debris flow sediment (Costa, 1984).

1.1.2 Geomorphic controls on debris flow initiation

Debris flows typically occur on steep (>25-30°) hillslopes mantled by low-cohesion soil or unconsolidated sediment (Iverson, 2014). Initiation sites are typically sparsely vegetated slopes that experience sporadic inputs of moisture, including the mountainous regions of the western United States (Costa, 1984; Iverson, 2014). Due to the importance of fluid forces discussed above, debris flow initiation is controlled largely by high inputs of water from rainfall or snowmelt and is therefore strongly dependent on local climate.

Although regional controls, including slope, elevation, and rainfall duration and intensity (Coe et al., 2008), are known to influence debris flow initiation, site-specific variables that control slope failure are not as well understood in the interior United States (Coe et al., 2014). Variables such as topography and hillslope material are thought to be important in influencing the exact location and abundance of debris flow activity when heavy rainfall and other regional conditions of susceptibility are met (Godt and Coe, 2007).

1.1.2 Debris flow hazards and landscape effects

Mass movements of all types can pose significant hazards to people and property (Costa, 1984; Iverson, 1997; Godt and Coe, 2007; Iverson, 2014). Delivery of large volumes of sediment and water to fluvial networks can pose additional hazards to human populations. Understanding the conditions of debris flow initiation and the downstream impacts of sediment transport can therefore significantly increase public safety and reduce property damage. Although the effects of events like debris flows and other mass movements on human populations are difficult to mitigate (Goode et al., 2012), management of buildings, infrastructure, and human activity that limits exposure to debris flows can reduce potential risk. In particular, identifying areas most likely to be inundated by debris flows or the coarse material mobilized on debris fans can provide a better understanding of debris flow risk across a landscape (Godt and Coe, 2007).

In addition to potential hazards posed by debris flows, slope failure and rapid transport of sediment shape the natural landscapes in which they occur by scouring debris channels (Stock and Dietrich, 2006; Schuster and Highland, 2007), destroying vegetation (Schuster and Highland, 2007), and transporting large volumes of sediment downslope (Godt and Coe, 2007;

Schuster and Highland, 2007). Sediment delivered by debris flows can also have a significant impact on the character and quality of rivers and streams; approximately 40 percent of the sediment reaching Rocky Mountain streams is derived from debris avalanches and debris flows (Schuster and Highland, 2007). This sediment is important in shaping the sediment budget and influencing the morphology of nearby fluvial networks; sediment disturbances caused by debris flows can produce large scale changes by reorganizing stream networks, forming massive sediment and wood deposits, and providing a wave of sediment input that can alter channel morphology, substrate size, and bed stability (Goode et al., 2012).

Assessing debris flow hazards is an inherently difficult task, as it requires predictions of where and when these highly stochastic events may occur, as well as how large they are likely to be (Iverson, 2014). Most hazards assessments rely upon empirical thresholds of rainfall duration and intensity in a region, or study of statistical patterns of historic debris flows. Both techniques require a sufficient dataset of debris flow occurrences through time in a given area. Hazard assessments in areas with infrequent or poorly documented debris flows, where standard empirical techniques are not as readily applicable, requires a detailed knowledge of the hillslope conditions that favor debris flow initiation, as well as the mechanics of flowing debris. Greater theoretical knowledge of debris flow susceptibility is an understanding that this study seeks to expand. Improved hazard assessment is particularly vital in areas where debris flows are infrequent, including much of the interior United States, where the hazards posed by debris flows are amplified because of the unpredictable nature of debris flows and the resulting lack of public awareness (Coe et al., 2014).

Debris flows and other natural hazards generate a conflict of needs for managers of national parks and public lands. While national parks aim to allow natural processes, including slope failures, to perpetuate and maintain wild landscapes (*Final Master Plan*, 1976), they must also balance these goals against the safety of staff and visitors. Identifying geomorphic variables that control debris flows in RMNP will inform management of park facilities and hazard mitigation by identifying where future debris flows are likely and what areas will be impacted downstream.

1.1.3 Debris flows in Colorado

Within the Southern Rocky Mountains of Colorado, debris flows are relatively rare (Caine, 1984). Small debris flows often occur in conjunction with localized, intense rainfall and flooding (Costa and Jarrett, 1981) or snowmelt floods (Costa, 1984; Wondzell and King, 2003). Conversely, larger events are often associated with wildfire (Cannon et al., 2001; Wondzell and King, 2003) or extreme rainfall (Menounos, 2000; Godt and Coe, 2007). Debris flows in Colorado may also be caused by anthropogenic activity including overtopping or piping through earthen dams or ditches (Costa and Jarrett, 1981; Rathburn et al., 2013; Grimsley et al., 2016).

Debris flows in the Colorado Front Range typically occur in small drainage basins with less than 8000 m^2 contributing area (Godt and Coe, 2007), because small convective thunderstorms drop proportionally larger volumes of water over small basins and because small basins are characterized by steeper, and therefore less stable, hillslopes (Costa and Jarrett, 1981). On previously undisturbed slopes in Colorado and in other areas with temperate climates, debris flows are often initiated as shallow landslides in unchannelized hillslope hollows (Iverson, 1997; Godt and Coe, 2007). In alpine areas burned by wildfire, or in poorly vegetated arid and semiarid

landscapes, initial slope failure usually occurs when hillslope material is eroded by overland flow (Godt and Coe, 2007). Debris flows triggered by the concentration of surface runoff or coalescing rills appear to pose greater hazards than do those initiated by landslides. This is likely because runoff-dominated slope failures are more susceptible to bulking (increased volume of the flow due to entrainment of sediment and debris) downslope of the initiation site, whereas landslide-related debris flows deposited a greater proportion of sediment as they traveled (Godt and Coe, 2007).

1.1.4 Debris flows and climatic forcing

Over-steepening of alpine hillslopes from glacial erosion increases hillslope susceptibility to debris flows and other forms of mass wasting (Eisbacher and Clague, 1994; Evans and Clague, 1994; Ballantyne, 2002b). As such, periods of paraglacial adjustment after retreat of glacial ice are characterized by increased debris flow frequency and magnitude (Evans and Clague, 1994; Ballantyne, 2002a, 2002b). Quaternary debris flow activity has been linked to climate degradation and amelioration through chronologic study in RMNP (Menounos, 2000) and elsewhere in the world (Solomina et al., 1994; Reid and Thomas, 2006). In the Colorado Rocky Mountains, patterns of debris flow activity reflect regional climate controls, including the presence and retreat of extensive glaciers and the ability of monsoonal weather systems to penetrate continental areas (Menounos, 2000). Enhanced summer precipitation after retreat of alpine glaciers in the Colorado Rocky Mountains (at the end of the Pinedale glaciation approximately 12 ka) likely controlled a widespread initiation of debris flow activity in the area, as evinced by lacustrine debris deposits in an alpine lake in central RMNP (Menounos, 2000).

This interpretation is supported by the observation that debris flows in RMNP are primarily initiated by summer convective storms (Costa and Jarrett, 1981; Menounos, 2000).

1.1.5 Effects of modern climate change on hazard assessment in the Southern Rocky Mountains

Atmospheric warming in the last few decades is particularly pronounced in the mountainous regions of the world (Huggel, 2009). Changes in the spatial and temporal pattern of debris flow initiation are likely to occur in the Front Range as climate patterns shift in the next few decades; more rain than snowfall is expected to occur in much of the western United States by the middle of this century (Klos et al., 2014). In addition to changing precipitation patterns and the timing and magnitude of storm events, changing climate patterns are likely to cause loss of vegetation and increased likelihood of wildfire in the Colorado Front Range (Goode et al., 2012). Such changes lower erosion thresholds and increase runoff, thereby increasing slope susceptibility to mass movement and increasing the total sediment load delivered to upland streams by debris flows and other episodic events. Understanding the conditions of debris flow initiation in the Front Range is therefore particularly important in developing infrastructure management and hazards mitigation plans in the future, when changes to global climate may limit the efficacy of statistical analysis of past debris flows in evaluating debris flow hazards.

1.2 September 2013 storm

An anomalous rainstorm in September 2013 triggered numerous debris flows in RMNP and over 1,100 debris flows throughout the Colorado Front Range (Coe et al., 2014). Figure 1.1 shows the RMNP study location and Figure 1.2 shows locations of all of the debris flow initiation sites identified using visual inspection of remote imagery (Coe, 2016, pers. communication).

1.2.1 Extreme rainfall

Nearly continuous rainfall occurred from 9-13 September across a 3430 km^2 area of the Colorado Front Range during the fall 2013 storm event, resulting in approximately 100-250 mm cumulative precipitation in eastern RMNP (Coe et al., 2014). Locally, cumulative precipitation exceeded 450 mm (Gochis et al., 2015). This storm delivered anomalously high cumulative rainfall late in the year, as is demonstrated by the high precipitation peak in the 2013 hyetograph from Estes Park relative to the same plot derived using data from the years 2007-2012 and 2014-2015 (Figure 1.3). In fact, this storm set a new record of greatest daily precipitation for the state of Colorado (Gochis et al., 2015). The calculated annual exceedance probability for this 24-hour precipitation record was estimated to be less than 1/1000 in some areas. Severe flooding, localized flash flooding, and mass movements that resulted from this storm caused eight fatalities and over $2 billion in damage (Gochis et al., 2015).

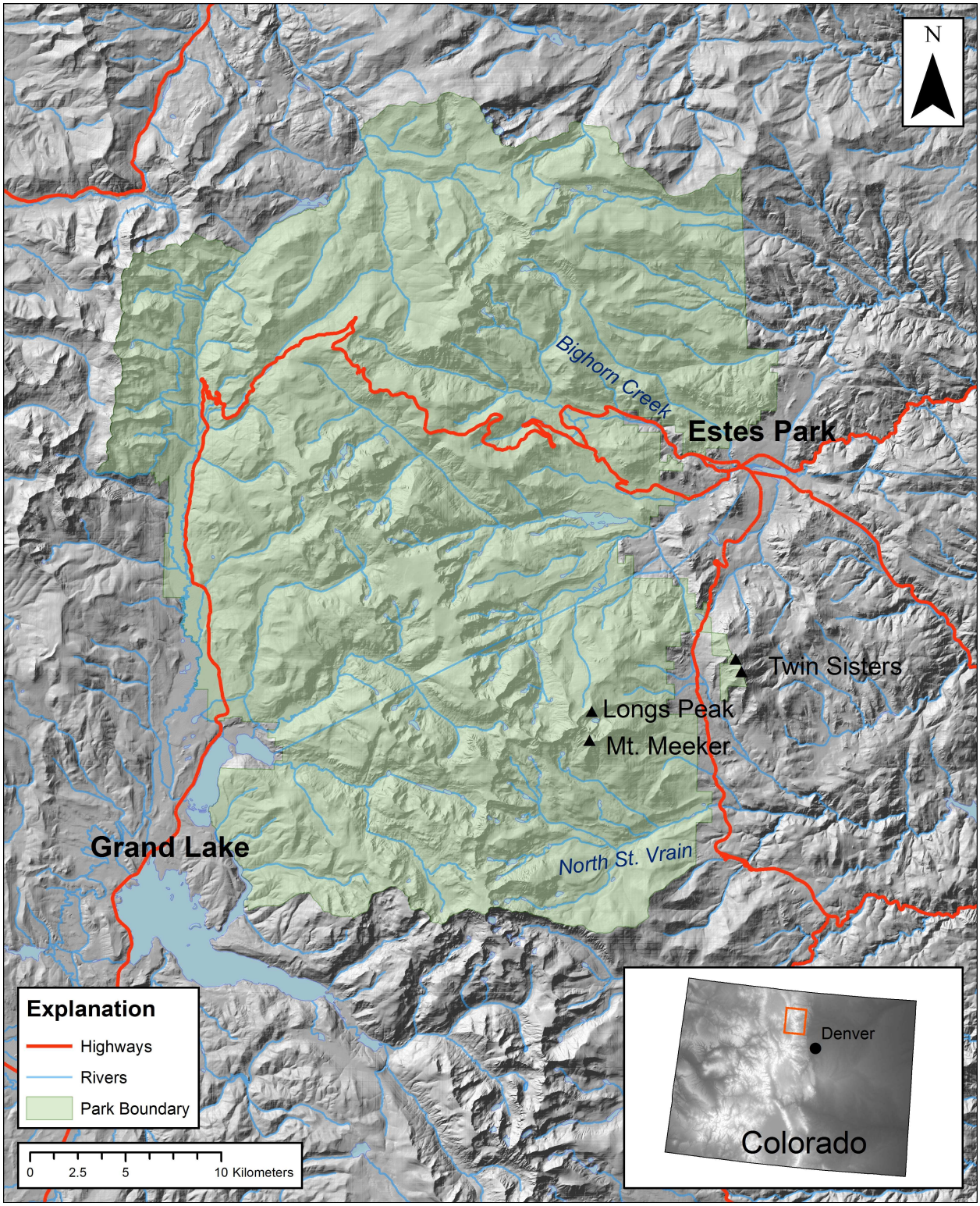

Figure 1.1. Map of the study area in RMNP. Notable locations (towns, peaks, and rivers) are labeled. The inset map shows the image extent within Colorado.

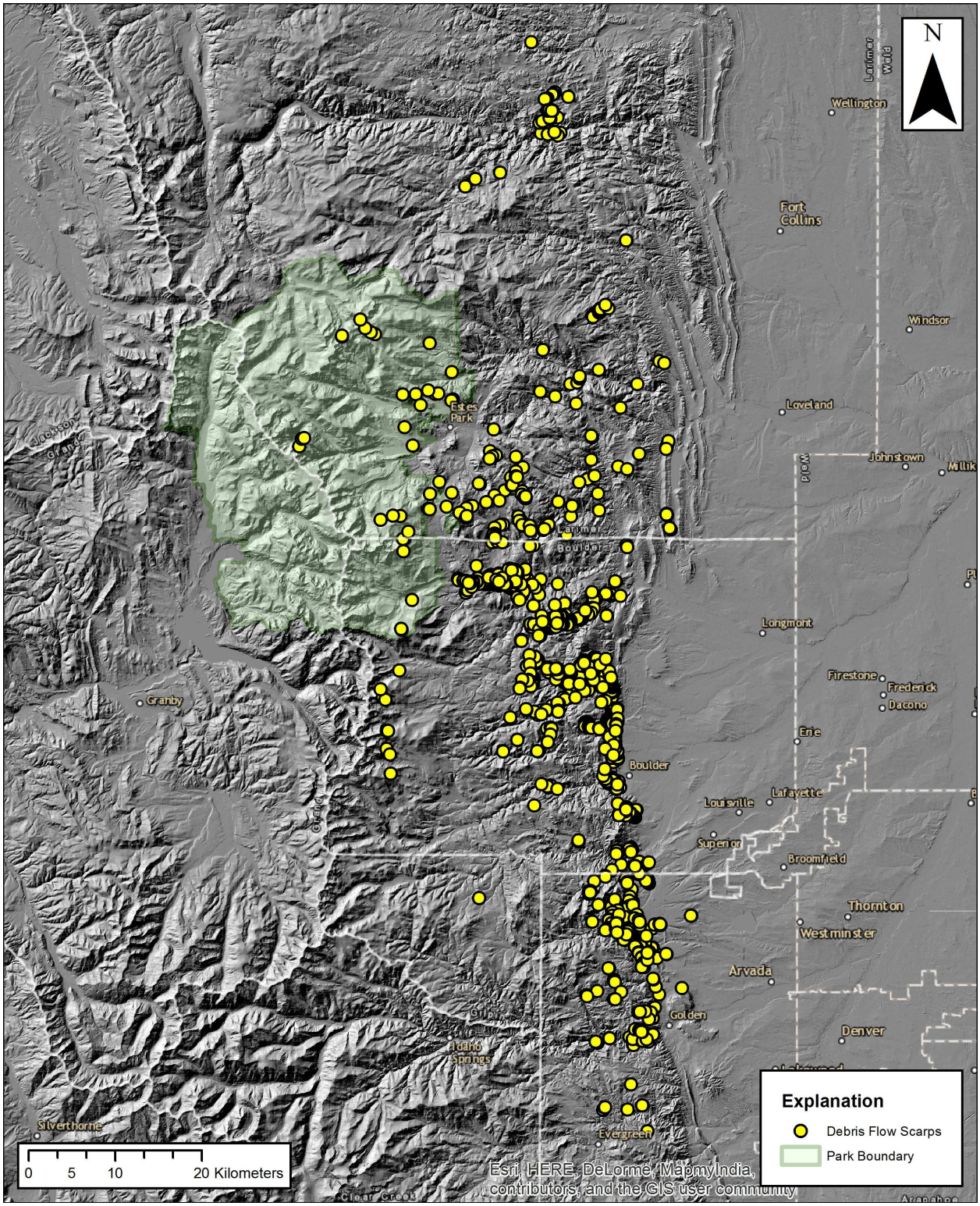

Figure 1.2. Location of debris flow initiation sites resulting from the anomalous 2013 rainstorm along the Colorado Front Range. Geospatial coordinates of debris flow sites as published in Coe et al., 2014, were provided by Jeffrey A. Coe via personal communication.

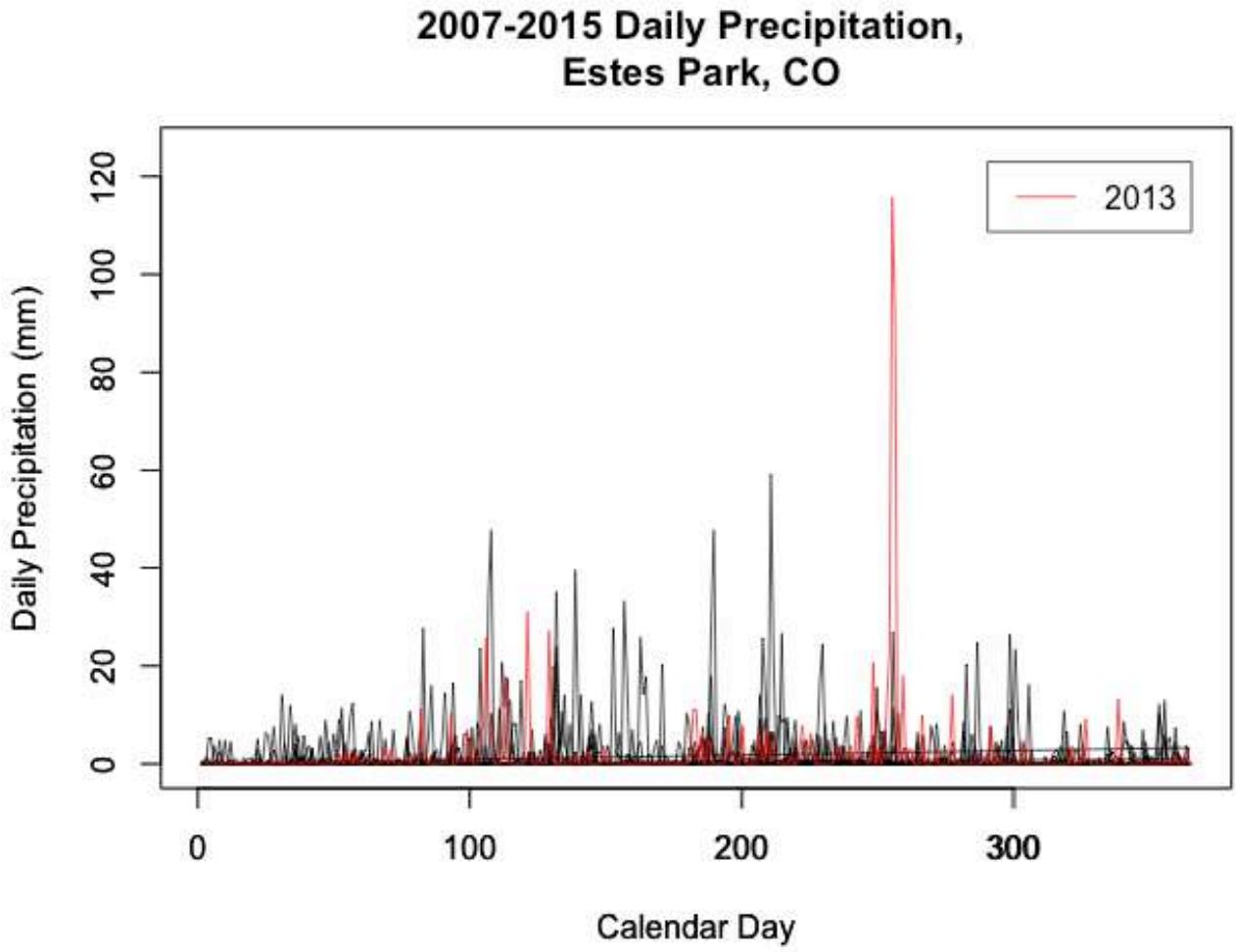

Figure 1.3. Hyetograph of daily precipitation in Estes Park, Colorado. Precipitation data from 2007-2012 and 2014-2015 are shown in black, and data from 2013 are shown in red. Data were obtained from the National Ocean and Atmospheric Administration Station gauge GHCND:US1COLR0767, accessed on March 26, 2015.

1.2.2 RMNP debris flows triggered by the 2013 storm

Of the numerous debris flows that occurred during this storm, over 10 medium to large-scale debris flows occurred in Rocky Mountain National Park, as well as several smaller slope failures (Coe et al., 2014; Gochis et al., 2015), causing extensive damage to buildings, roads, and trail infrastructure within and adjacent to the park. Most notably, an historic ranger station built on a former debris fan was threatened by one of the 2013 flows near Bighorn Creek, underscoring the

potential for ongoing hazards in this area. Debris flows within RMNP that were initiated by the 2013 storm are also of particular concern and warrant detailed investigation because they delivered significant sediment loads to upland streams (Schutte et al., 2014). The extensive nature of debris flow initiation following the 2013 storm provides a valuable opportunity to better understand the controls on debris flow initiation in RMNP.

During the 2013 storm, debris flows within RMNP occurred primarily in the eastern portion of the park. Initial assessment of September 2013 debris flows directly following the event found that debris flows occurred across a wide range of elevations (high plains to alpine climatic zones) and in soils formed on multiple lithologic units (Godt et al., 2014). Initial surveys of debris flow locations after the storm indicate that they occurred primarily on south and east-facing slopes greater than 25° and that most flows occurred at elevations above 2600 m, the elevation threshold where snowfall strongly influences fluvial systems (Coe et al., 2014). Because cumulative rainfall was relatively uniform over a broad area (150-250 mm where most large flows initiated in RMNP), and debris flows occurred on steep slopes at similar elevations (2500-3000 m), this event allows for independent analysis of other controls on debris flow occurrence. The 2013 debris flows selected for detailed study are all located in the eastern portion of RMNP.

1.3 Study area

This study focuses on debris flow initiation within and immediately adjacent to RMNP. The national park is a high-relief landscape located in the Colorado Front Range of the Southern Rocky Mountains (KellerLynn, 2004) and is characterized by dynamic environments that extend from the continental divide to the mountain towns of Estes Park and Grand Lake. The study

region encompasses alpine, subalpine, and montane vegetation zones as defined in the Colorado Front Range (Sibold, Veblen, and Gonzalez, 2006; Birkeland et al., 2003).

1.3.1 Climate

Under normal conditions, precipitation patterns throughout the Rocky Mountains of Colorado are strongly controlled by elevation (Colorado Climate Center). Mountainous areas, including RMNP, receive most of their yearly precipitation as snowfall during the winter months. At elevations above approximately 2,400 m, melting of the accumulated snowfall is minimal until spring, and fluvial systems in the Front Range are strongly snowmelt-dominated. During the summer months, particularly in July and August, convective thunderstorms generate high intensity local precipitation and occasionally cause severe flash floods in mountain catchments.

1.3.2 Underlying geology

In the study sites in the eastern portion of RMNP, the underlying bedrock primarily consists of crystalline rocks of Proterozoic age (Braddock and Cole, 1990). Underlying lithologies at the study sites include the Silver Plume Granite, a monzogranite to syenogranite unit from the middle Proterozic, and a biotite schist unit from the early Proterozoic. These units are typically the dominant near-surface lithology on steep hill slopes in the park and are characterized by similar geochemistry; most soils in the Colorado Front Range are therefore derived from coarse-grained parent material high in feldspar, quartz, biotite, and hornblende (Birkeland et al., 2003). Valley bottoms throughout RMNP are typically composed of alluvial deposits of Holocene and upper Pleistocene age and glacial sediment of upper Pleistocene age, including till from the Pinedale Glaciation (30-12 ka) and the Bull Lake Glaciation (150-130 ka) (Madole et al., 1998).

In addition to depositing large volumes of sediment, Pleistocene glaciers eroded the steep-walled valleys that characterize the modern landscape. These over-steepened valleys contribute to the instability of hillslopes in RMNP and increase the importance of gravitationally-induced sediment transport, including debris flows and other mass movements, in controlling landscape characteristics and sediment budgets (Madole et al., 1998; Anderson et al., 2015).

2. HYPOTHESES AND OBJECTIVES

The main goals of this research are to identify the primary site-specific controls (Figure 2.1) on debris flow initiation in the Colorado Front Range and to quantify the frequency of these events at susceptible sites. Such analysis is intended to determine whether the 2013 debris flows were low probability events, precipitated by anomalous hydroclimatic conditions, or whether they are likely to recur in predictable locations on a human timescale. Potential controls on debris flow initiation, including both regional and site-specific controls, are outlined in Figure 2.1. Specific project hypotheses and objectives are described in the sections below.

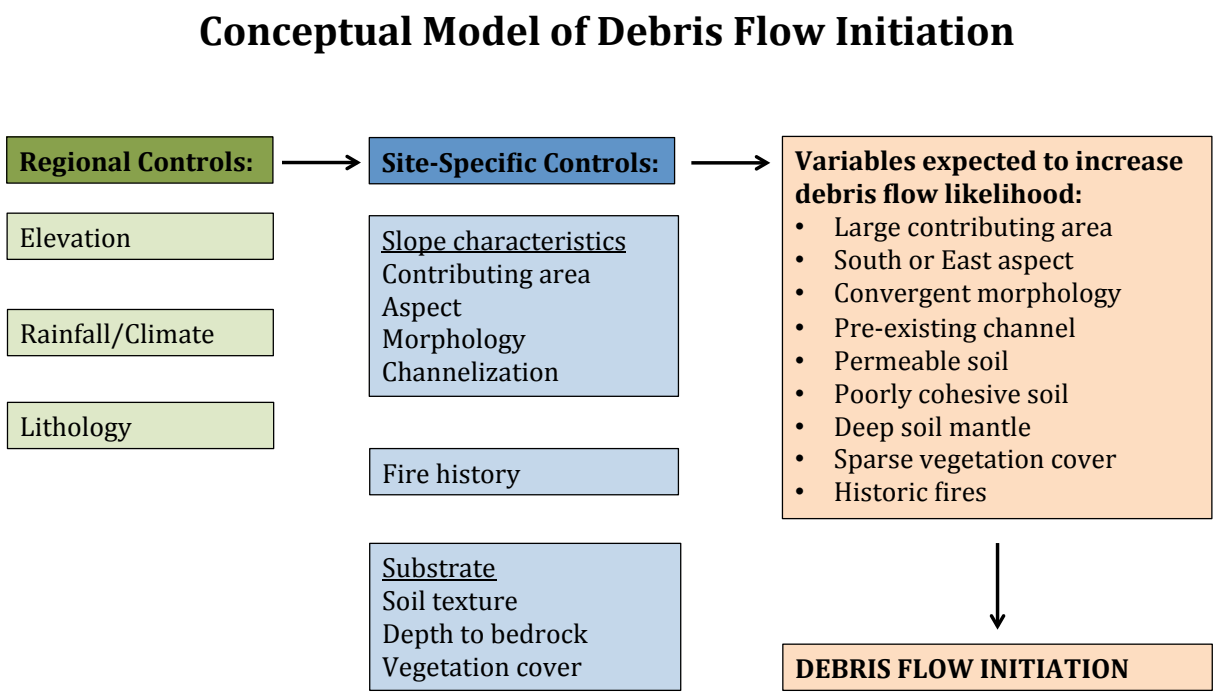

Figure 2.1. Conceptual model illustrating controls on debris flow initiation. Regional controls are consistent between the study sites. This research focuses on determining the dominant site-specific controls that increase the likelihood of debris flow initiation, including slope characteristics, substrate, and fire history. Slope morphology is a term used in this thesis to describe both the contributing area and relative degree of convergence of the hillslope.

2.1 Hypotheses

1. Slope geometry (concavity/convexity), subsurface bedrock topography and substrate characteristics are dominant site-specific controls on debris flow initiation, as colluvial hollows and subsurface depressions accumulate unconsolidated sediment.
2. Fire history may outweigh slope characteristics in initiating debris flows.

2.2 Rationale

Initial field observations indicated that debris flows within RMNP occurred at locations where unconsolidated sediment provided sufficient source material. As noted by Godt and Coe (2007), debris flows initiated by shallow landslides in the Colorado Front Range often occur in colluvial hollows (topographic concavities that are able to collect sediment) on steep hill slopes. The material within colluvial hollows provides abundant unconsolidated source material. Similarly, hillslopes in the Colorado Front Range that generated debris flows by rilling were typically concave (Godt and Coe, 2007). Such concavity would more effectively accumulate both surface and subsurface flow, increasing saturation of slope materials.

In addition to morphological controls, debris flows occur most frequently in low-cohesion substrates, as such material is less able to resist the gravitational and shear forces that initiate downslope movement (Iverson, 1997, 2014). Because soil texture and root properties influence soil cohesion, soil texture and dominant vegetation type are also likely controlling variables on debris flow initiation. In particular, the percent silt/clay and the percent organics strongly influence hydrologic properties of soil because these textural characteristics influence the surface

area per unit volume (Birkeland, 1999) and would therefore influence the saturation and pore pressure conditions of a hillslope during a large rainfall event such as the 2013 storm.

In addition to the inherent geomorphic and substrate properties on a particular hillslope, severe wildfires can reduce the influence of root cohesion and contribute to episodic slope failures (Wondzell and King, 2003; Goode et al., 2012). Furthermore, soils experience altered hydrologic properties following wildfire, including reduced interception of rainfall by vegetation (Swanson, 1981), reduced transpiration of soil moisture (Swanson, 1981; Megahan, 1983), and increased surface erosion (Swanson, 1981; Wondzell and King, 2003; Nyman et al., 2013). These post-fire substrate characteristics may therefore increase the susceptibility of a hillslope to failure and mass movement regardless of other slope characteristics.

2.3 Other objectives

In order to characterize the spatial and temporal occurrence of debris flow initiation in RMNP, the following objectives seek to describe historic debris flows and assess areas that may be susceptible to debris flow initiation in the future. The objectives listed below are intended to inform management of park lands and structures through analysis of debris flow frequency at susceptible sites and by identifying other areas that may experience future mass movements.

i) Determine debris flow chronologies at sites with recurring debris flows.
ii) Conduct park-scale landscape analysis to identify other areas susceptible to debris flows based on geomorphic variables.

3. METHODS

Multiple methods were employed in the field and in the laboratory to investigate 2013 debris flow initiation and debris flow frequency in RMNP. These methods included field surveys, comparisons of debris flow sites with control sites, spatial analysis of topographic imagery, field trenching of debris flow deposits, and field sampling and laboratory analysis for geochronologic control. In addition, statistical analyses were conducted to evaluate significance of several potential geomorphic controls on debris flow initiation.

3.1 Debris flow surveys

Reconnaissance fieldwork was conducted in summer 2014 to characterize the general morphology and magnitude (estimate as dimensions of the failure scarp and flow path) of debris flows that initiated in the September 2013 storm. Seven debris flow deposits were identified and surveyed in 2014. This sample was expanded to include four additional debris flow sites identified in summer 2015. Using a laser rangefinder, debris flow deposits were surveyed by measuring the horizontal and vertical distance from the channel floor to the top of the debris flow levee on either side of the channel (Figure 3.1). Two of the surveyed debris flows were not clearly channelized; in these cases, survey points were taken from the middle of the debris flow path to the deposit margins in order to map the planform of the flow. Distances collected using the laser rangefinder are reported to tenths of a meter with an accuracy of $\pm$ 0.3 m ("LTI TruPulse 360 / 360B User's Manual 2nd Edition," 2009). Measurements were taken at intervals of approximately 20-40 m along the channel except where extremely steep terrain limited safe access. The spatial location of each measurement was collected using a handheld GPS unit. In locations where the debris flow path diverged for some distance around a ridge of unaltered

hillslope, both sub-channels were measured independently for a more accurate description of the channel profile and morphology. Some of the debris flows studied were not surveyed along their entire extent due to unsafe conditions accessing the channel, including most of the length of the debris flow that initiated on the eastern slope of Mt. Meeker. At these sites, supplementary width measurements of the debris flow channel and deposit were calculated from Google Earth Imagery.

Figure 3.1. Survey of a debris flow in Black Canyon (northern slope) using a laser rangefinder.

At each site, field observations were used to delineate zones of erosion, transportation, and deposition. Maximum transport distance of each debris flow was estimated in Google Earth by measuring the horizontal distance between the debris flow scarp and either 1) the distal portion

of the debris fan or 2) the point where the debris flow entered an established stream channel. A GPS point was also collected at the headscarp of each debris flow, and the laser rangefinder was used to estimate the horizontal and vertical distance from the top of the scarp to the break in slope at the base of the scarp.

The locations of surveyed debris flows are described in greater detail in the sections below.

3.2 Slope characterization

Slope variables including soil depth, soil texture, contributing area, slope convexity/concavity, primary vegetation type, and vegetation density were measured at 11 debris flow sites and 30 control sites within RMNP. Statistical tests for significance were then used to determine the influence of these potential geomorphic controls on debris flow initiation (Figure 2.1). Debris flow sites and control sites are mapped in Figure 3.2.

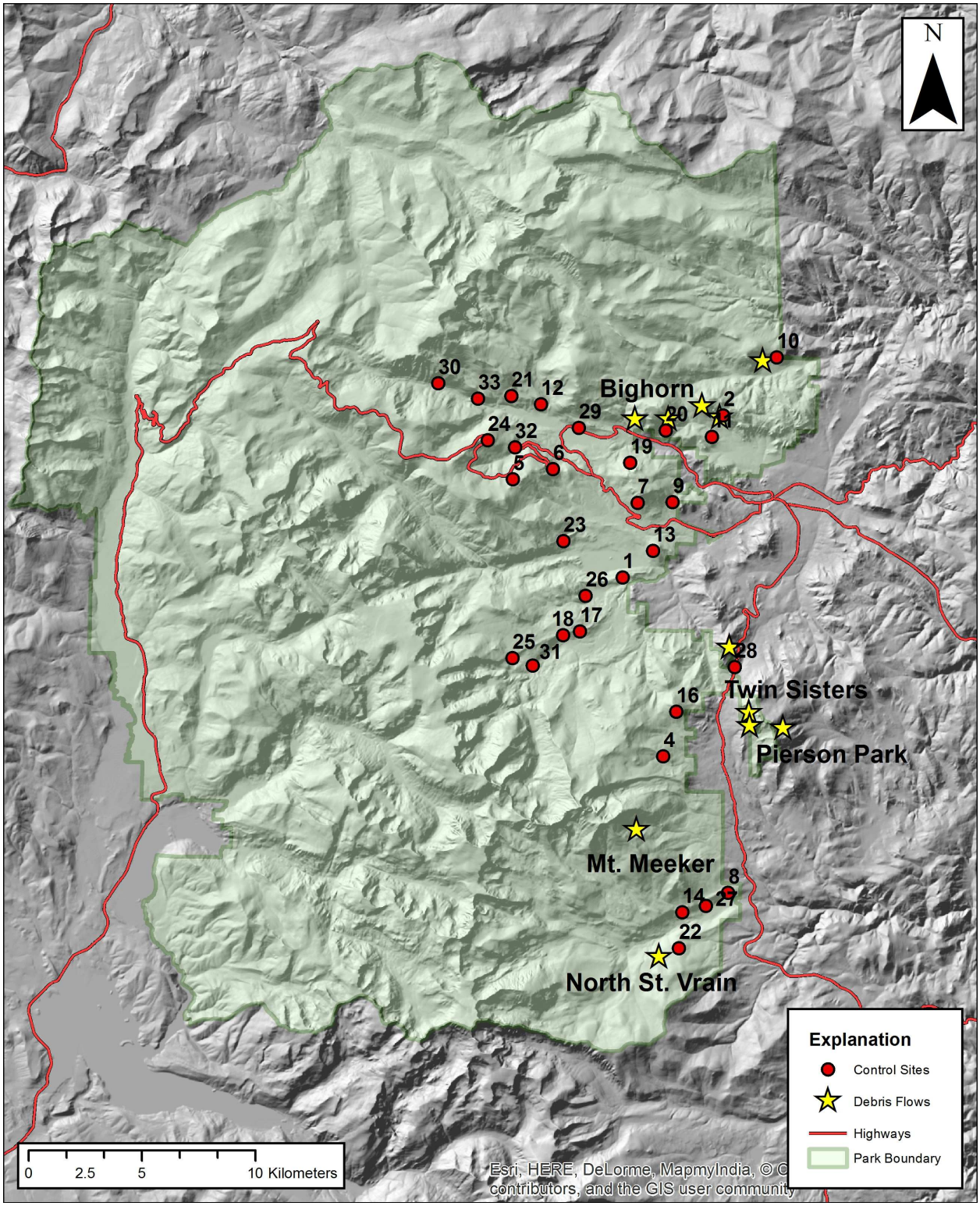

Figure 3.2. Locations of debris flows and control sites in RMNP. The names of several notable debris flows are included for discussion in the following sections.

3.2.1 Site selection

Eleven debris flow sites were located by personal observation in the field and using Google Earth imagery collected after September 2013. Another study (Coe et al., 2014) identified numerous additional debris flows throughout Colorado Front Range, including several small debris flow scarps within RMNP. Coe et al. (2014) relied primarily on visual inspection of remote imagery across a large area (Coe, pers. communication). Upon detailed review of the debris flow scarps identified within and near RMNP, the debris flow sites identified in Coe et al. (2014) include several very small debris flow scarps as well as areas of fluvial erosion and undisturbed hillslopes. The majority of the debris flows analyzed in this thesis were larger features that could be identified individually and that delivered sediment to main river channels. A later publication (Gochis et al., 2015) shows an updated dataset that more closely matches the number and location of debris flows identified in RMNP in this thesis. Each of the 11 debris flow sites used in this study were accessed in 2014 and 2015 for confirmation and field measurement.

Control sites on hillslopes that did not fail were selected by generating raster data defining slope angle, slope aspect, and elevation for the study region based on 10 m DEM imagery. These topographic data were extracted for each of the known debris flow scarp locations (identified during reconnaissance fieldwork in summer 2014). Basic statistical summaries (mean, median, standard deviation, and general distribution type) were then calculated for each slope variable. Using the raster datasets, 32 control sites were then selected manually to achieve an unbiased sample of slopes with a similar range of slope angles, aspects, and elevations as those that characterized the debris flow sites. Manual selection of sites allowed for desired control site conditions to be met while ensuring that each site was located near a road or hiking trail for

accessibility. Bias introduced from manual site selection was limited, as control sites were selected remotely using categorical raster data. The group means and standard deviations for each slope angle, slope aspect, and elevation were compared between the debris flow sites and control sites to ensure a similar distribution of data. Geospatial coordinates for each of the control sites were recorded to five decimal places.

Using a handheld GPS to locate each site, the control sites were accessed in the summer of 2015 for field measurement and sample collection. A few of the control site coordinates could not be accessed due to steep rock outcroppings. In these cases, measurements were collected at an alternate site chosen in the field using best judgment to find a site as near as possible to the pre-selected coordinates. At each control site, the field-corrected location of slope measurements was recorded using a handheld GPS for future calculation of topographic variables. Soil depth, soil texture, dominant vegetation type, and vegetation prevalence were measured according to the techniques described below.

3.2.2 Soil depth, soil texture, and vegetation

At the 30 control sites and 11 debris flow sites, soil depth was measured using a 1.5 m probe with decimeter markings (Figure 3.3A). At each site, depth measurements were collected at 1 m intervals along a 20 m tape stretched perpendicular to the slope (Figure 3.3B). At debris flow sites, this tape was positioned approximately 2-5 m above the debris flow scarp and was centered around the failure surface. In order to minimize the influence of rocky soils, recorded depths at each meter along the tape indicate the deepest measureable soil depth (where the probe met refusal) found within 0.3 m of the tape.

A. **B.**

Figure 3.3. Soil depth measurements at two control sites in RMNP. Soil depth was measured using a 1.5 m probe at 1 m intervals along a 20 m tape.

Vegetation characteristics were assessed along the same 20 m tape used for soil depth measurements. Primary vegetation type was classified as coniferous forest, brush, or grasses and herbaceous plants. The vegetation density was then estimated by counting the number of individual trees or shrubs standing within 0.3 m of the 20 m tape. Where applicable, the tree species present and their relative prevalence were also recorded.

Soil texture was assessed for soil samples collected at control sites using sieve separation. Each sample was collected using a hand auger with an 8 cm diameter bit until the auger met refusal, usually due to a large tree root or rock. In the lab, wet samples were split using a soil splitter to create a reserve sample, weighed while still field-damp, oven-dried at 100° F for 24 hours, and then weighed again to calculate the percent water in each sample. Masses were recorded in grams to two decimal places. Any large organic material was removed by hand and weighed, and

the remaining sample was then sieved on a Rotap for 5 minutes using sieves of -2ϕ, -1ϕ, 0ϕ, 1ϕ, 2ϕ, and 4ϕ diameters. Each portion of the original sample was then weighed to generate a grain size distribution using the percent mass in each grain size class. The percent gravel (-2ϕ to -1ϕ), percent sand (-1ϕ to 4ϕ), and the percent silt/clay (>4ϕ) were then calculated for each sample based on the total sieved weight. Soil texture descriptions include percent organics, percent gravel, percent sand, percent silt/clay, and percent water. Percent water in each sample, however, reflects a number of temporal variables related to sample collection times that have not been accounted for in this study, including season, recent precipitation, and time of day. As such, percent water is not considered a diagnostic variable in the data analysis.

Samples were also collected and processed according to the methodology described above at each of the debris flow sites for textural comparison with control site soils. Debris flow samples processed for textural analysis were collected from undisturbed soils approximately 2-5 m above the debris flow scarp to ensure that collection methodology was consistent at both site types.

At each debris flow site, 2-3 additional soil samples were also collected directly from the scarp at increments of 10 cm, 1 m, and 2 m below the top of the scarp where exposure was sufficient. The soil samples collected from the scarp face were stored as a physical record of soil texture in the debris flow scarps during the course of this study. Because samples collected from scarp faces did not follow the same methodology as those collected from debris flow sites, however, these samples were not analyzed for textural comparison with control sites.

3.2.3 Topographic characterization

At each of the 41 study sites, slope morphology was classified based on field observations. First-order classifications indicated whether the study site was characterized by convergent topography or planar/divergent slope morphology. Sites considered "convergent" were further classified according to whether a colluvial hollow was present at or immediately above the site. Colluvial hollows were identified where a small concavity (10-50 m across) was present in the hillslope. Bedrock outcrops typically defined the colluvial hollows identified in this study by forming the top and sides of small, densely vegetated bowls in the slope topography.

After the conclusion of fieldwork, slope morphology was more precisely quantified for each of the study sites. Slope variables including contributing area and slope curvature were computed using 10 m DEMs. Elevation data were used to generate a raster dataset of flow accumulation, which was then used to generate polygons delineating drainage area to each site such that contributing area could be calculated. The drainage area polygons were manually verified against topographic maps of each hillslope to ensure that reasonable areas were calculated. Two metrics of slope curvature were calculated as raster datasets for the study region, including a measure of slope concavity both parallel to the slope (planform curvature) and a combined measure of concavity parallel and perpendicular to the slope (general curvature). Slope curvature, a relative score of concavity/convexity, was considered a proxy for the degree of slope convergence. The value of both curvature scores was extracted for each study site.

Curvature is calculated by finding the second derivative of elevation data for a given cell and its eight neighbor cells. Using a 10 m DEM, it is therefore a moving average score for a 30 m

square area. To characterize curvature over a larger area, planform curvature was also calculated for a resampled 30 m DEM, such that the curvature score was calculated for a 90 m square area.

3.2.4 Fire history

Extensive ecological studies previously conducted in and near RMNP have identified areas that have experienced wildfire since the middle of the last century (Sibold et al., 2006; Buechling and Baker, 2004). Using the spatial datasets compiled in these studies, the date of the most recent fire, or the lack of known fire at each of the studied debris flow sites and control sites was recorded. In order to categorize the degree of fire effect on the hillslopes, each site was categorized based on the time since the most recent known fire. Although forest recovery is highly variable depending on fire severity, elevation, and other factors, tree density in mixed Ponderosa pine/Douglas-fir forests in parts of the Rockies typically reach pre-fire levels within 60-100 years after a severe fire (Baker, 2009, p 241). Fires that occurred no more than 60 years before 2013 (1953 or later) were therefore categorized as "recent" fires that likely continue to influence hillslope hydrology and sediment transport on the affected hillslopes. Sites that had not experienced fires within the 60 years before 2013 were classified as hillslopes that had not experienced recent fire during the storm. Because no study sites have experienced wildfire within the last 10-20 years, the short term effects of fire on debris flow initiation could not be assessed in this study.

3.3 Debris flow chronology

The Bighorn debris flow site (Figure 3.2 above) was selected for detailed chronologic study because of the presence of older debris flow deposits and the proximity to park buildings and infrastructure. Older debris deposits were also identified near the distal portion of the debris flow path at the Mt. Meeker site. Unlike the Bighorn site, however, the old deposits at Mt. Meeker could not be conclusively linked to a single source area and were therefore not included in the geochronologic assessment described below.

Older debris flow deposits at the Bighorn debris flow site include an extensive debris fan below the 2013 debris deposit and several discontinuous debris flow levees. Multiple geochronologic techniques were employed to establish both relative and numeric ages of older debris flow deposits at the Bighorn debris flow site, including trench excavation to expose the stratigraphy in the old debris fan, dendrochronology, lichenometry, radiocarbon dating of wood samples collected from the exposed trench and from old debris deposits, and 10-Berylium (^{10}Be) radionuclide analysis conducted on boulders in old debris flow levees. Figure 3.4 shows the Bighorn site and sample locations, which are described in the following sections.

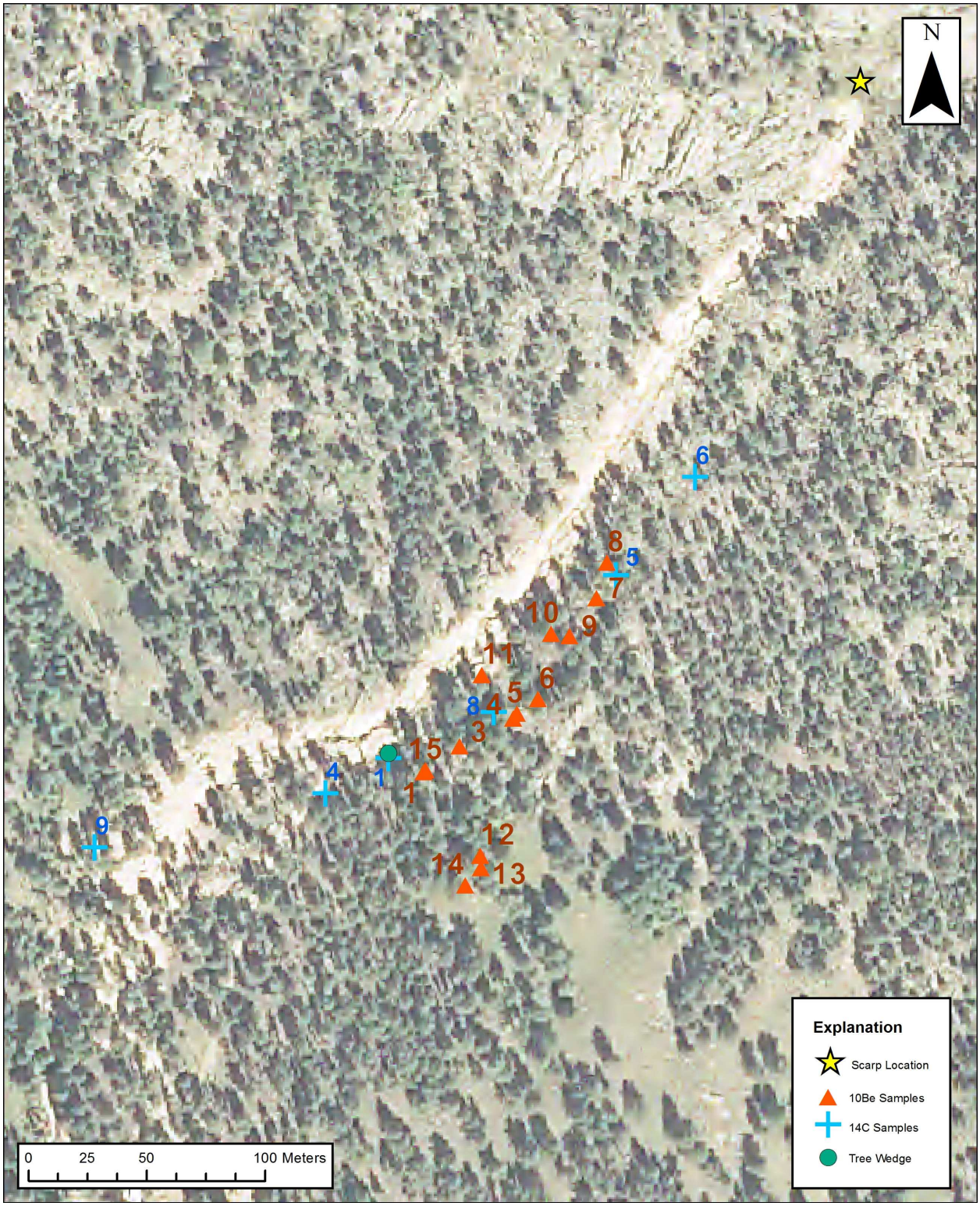

Figure 3.4. Bighorn debris flow site and sample locations. ^{14}C sample number nine (bottom left) was collected from an excavated trench in the pre-existing debris fan.

3.3.1 Deposit identification and mapping

Older debris flow levees were first identified by finding small-scale ridges (1-3 m wide with variable lengths) comprised of aligned and imbricated boulders in the Bighorn Creek drainage that are approximately parallel to the 2013 debris flow channel. Debris levees are composed of poorly sorted debris, with boulders and cobbles suspended in a fine matrix. Deposits farthest outset from the 2013 debris flow path, however, are not characterized by distinct ridges and are weathered such that no fine debris remains and the deposits consist entirely of aligned boulders. Field observations of relative levee diffusion (gradual smoothing and erosion of fine material through time) and surficial weathering of boulders were noted for each of the old debris flow levees at the Bighorn site. Using a high-resolution GPS, crests of levee deposits were mapped to determine downslope extent and spatial relationships to other deposits, and were interpreted to indicate relative ages. The 2013 debris flow levees and the outline of the 2013 debris fan were also mapped to show spatial relationships of older deposits to the 2013 channel and levees.

3.3.2 Stratigraphic analysis

In August 2015, a 4 m long, 1 m deep trench was excavated in the distal region of the old debris fan near Bighorn Ranger Station for stratigraphic analysis. Grain size, sorting, color, thickness, and compaction of the exposed soil and sediment deposits were described, photographed, and interpreted in the field. In addition, one sample of unidentified organic material was collected for radiocarbon analysis, described in section 3.3.3 below. The location of the trench is indicated by the position of ^{14}C sample number nine in Figure 3.4.

3.3.3 Radiocarbon analysis

At the Bighorn debris flow site, pieces of organic material were found in exposures of old debris deposits, including one sample of decomposed plant matter in the excavated trench and two samples that were exposed in the sides of the 2013 debris flow channel. Two wood samples were also collected from old debris flow levees where large pieces of wood were pinned between and below boulders in the levees (Figure 3.5). All samples were sent to DirectAMS for radiocarbon analysis to determine the age of the events that buried organic material.

Figure 3.5. Wood sample collected in an old debris flow levee at the Bighorn debris flow site. The sample was pinned between boulders, indicating that it was emplaced during the debris flow event that formed the levee, and exhibited spear-like fragmentation that characterized other observed pieces of wood trapped between boulders in the 2013 deposit.

3.3.4 Aerial photos

Aerial photos from flights in 1937, 1965, 1969, 1987, and 2001 were accessed to identify debris flows in RMNP that have occurred during the historic record. Although the resolution of available photos limits the confidence with which debris flows can be recognized, probable debris flows were recorded with an approximate confidence (high, moderate, poor) that the feature was correctly identified in the historic imagery. The date of photos in which debris flows were identified was used to constrain the age of each event. Debris flows in the historic record were then tallied for the RMNP region to indicate approximate frequency of events within the park since 1937.

3.3.5 Lichenometry

Diameters of a large sample (>100) of the largest lichen colonies on a geomorphic feature can be used to date the surface using a regional growth curve. This method has been successfully used to date seismically-induced mass movements (Bull, 1996). Previous study (Benedict, 1967) established a growth curve for the lichen species *Rhizocarpon geographicum* in the Colorado Front Range. Due to local site conditions, however, no individuals of species *R. geographicum* were identified at the Bighorn study site, so this method could not be used to date old debris deposits. As an alternative, the largest colony diameters of three other lichen species (Figure 3.6) were measured on boulders from two old debris flow levees. Although growth curves have not been established for these species, average colony diameter on each levee may indicate relative ages.

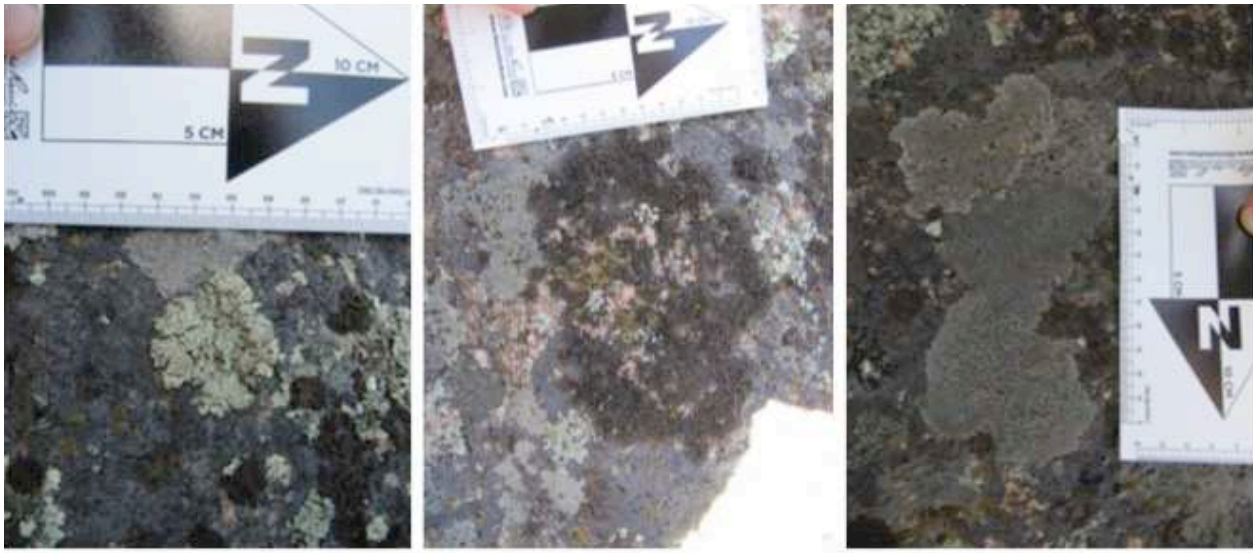

Figure 3.6. Three lichen species measured for relative dating at the Bighorn debris flow site.

3.3.6 Dendrochronology

Scarring of standing trees can also record precise evidence of mass sediment movements, particularly where multiple trees corroborate a single age of a large event (Stoffel et al., 2013; Grimsley et al., 2016). At the Bighorn debris flow site, one ponderosa pine that was felled in the 2013 event showed evidence of older scarring. Two cross-sectional wedges were cut through the older scarred portion of the trunk for age analysis. The wedges were then sanded and polished and the number of tree rings between the outermost ring (the 2013 growth ring) and the undamaged wood in the center of the tree were counted to indicate years since the scarring occurred. Although a single scarred tree cannot conclusively indicate a mass movement event, the age indicated in this analysis may be used to corroborate ages determined using other geochronologic techniques.

3.3.7 ^{10}Be radionuclide analysis

Cosmogenic radionuclide analysis has been successfully implemented to date a limited number of mass movements, despite complications including potential inherited exposure ages and post-event mobility of boulders (Mackey and Quigley, 2014; Granger et al., 2013). Assuming that the debris flow removes sufficient material from a rock or boulder surface to effectively reset the exposure age, the rate of cosmogenic bombardment and the relative concentration of ^{10}Be in quartz grains can be used to calculate the exposure age of depositional surfaces where the surface is younger than several ^{10}Be half-lives of 1.389 $\pm$ 0.014 m.y. (Granger et al., 2013). At the Bighorn debris flow site, 14 rock samples were collected from boulders in three old levees, including the two levees analyzed using lichenometry as well as the mapped levee segment farthest outset from the 2013 debris flow channel (and therefore oldest). (Figure 3.4 above).

Each sample was collected from large, apparently stable granitic boulders to minimize the likelihood that they had rolled downslope since deposition or that they had been subject to transport by other surficial processes. Sample sites were also chosen where the material for collection was positioned on the top of the boulder to minimize shielding effects from the boulder itself. The location of each sample was recorded using a high-resolution GPS. Samples were then collected using a handheld sledge and chisel. At each sampling location, additional sample data were collected including 8-10 measurements of inclination and bearing to the horizon, slope of the boulder surface, and the maximum sample thickness. Shortly after collection in the field, samples were cut to the desired dimensions using a rock saw.

Rock samples were processed mechanically and chemically for ^{10}Be analysis at the Purdue PRIME lab by the author according to PRIME lab protocols, using the Nishiizumi et al. (2007) ^{10}Be standard. Exposure ages were calculated from AMS Be concentration data according to the CRONUS online calculator, version 2.2 (Balco, 2008) using the global production rate latitude, longitude, and elevation recorded with the GPS unit in the field, maximum sample thickness measured for each sample, approximate sample density based on the average density of granitic rocks (2.65 g/cm^3), and a shielding correction calculated using the CRONUS calculator, which uses angle to horizon data measured at each sampling concentration.

4. RESULTS

Data were analyzed using spatial and statistical techniques to test the research hypotheses, including comparisons of site variables at debris flow sites and control sites, compilation of geochronologic age data, creation of feature maps, and processing of survey data.

4.1 Debris flow surveys

The surveyed debris flows demonstrated variable morphologies, including differences in scarp dimensions and variation in channel lengths and cross-sectional dimensions. Each of the 11 debris flow sites is shown in Figure 4.1 on the following two pages. Surveyed debris flow dimensions of the 11 debris flows are summarized in Table 4.1.

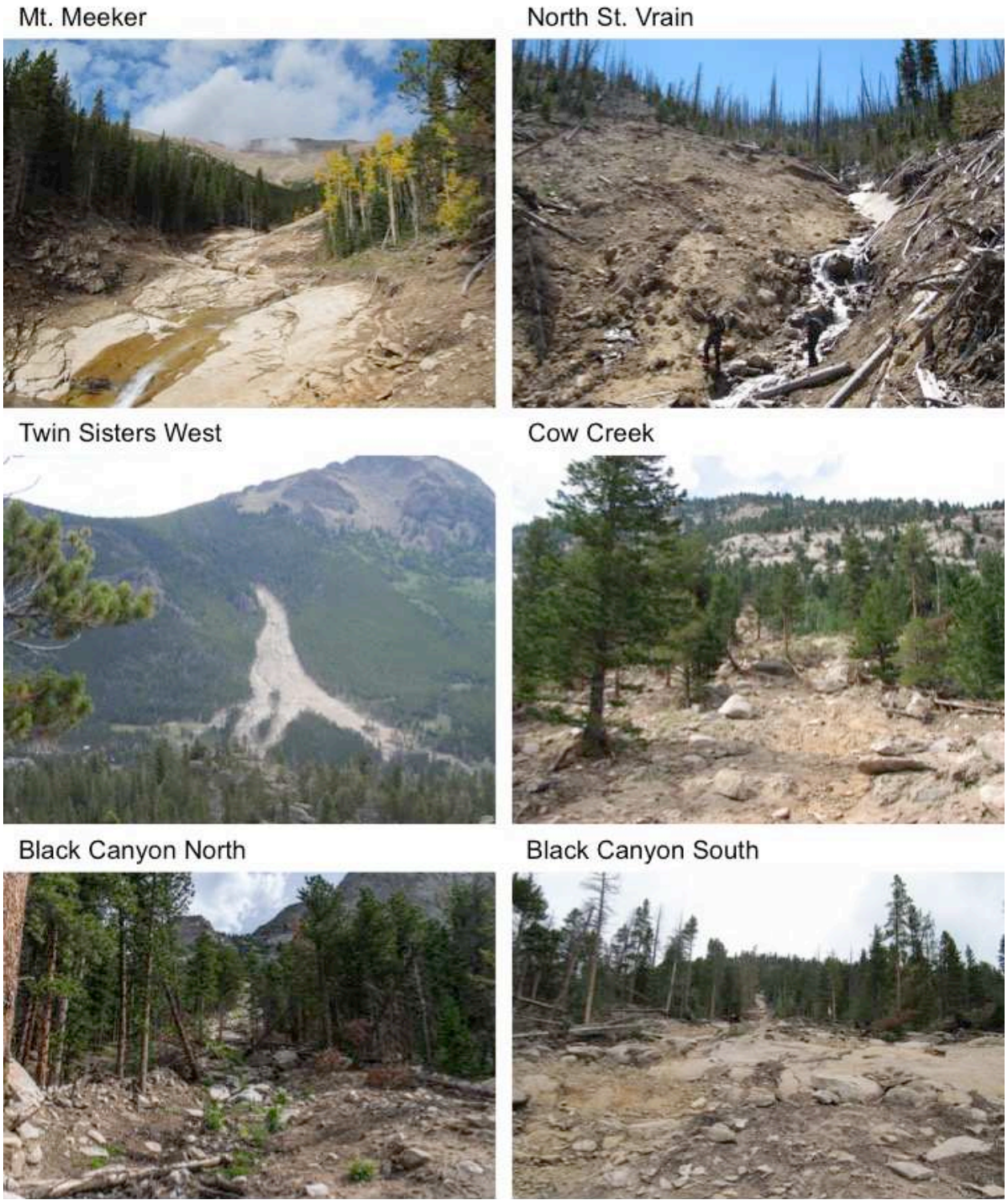

Figure 4.1 A. Debris flows surveyed in RMNP during this study.

Figure 4.1 B. Debris flows surveyed in RMNP during this study.

Table 4.1. Dimensions of surveyed debris flows.

Number	Site name	Scarp width (m)	Scarp height (m)	Transport distance (km)	Max flow width (m)	Max channel depth (m)	Failure volume (m^3)
1	Mt Meeker	17.8	3.9	4.35	38.7	8.5	2.59×10^3
2	North St Vrain	29.9	11.6	0.74	18.5	5.2	2.17×10^4
3	Twin Sisters West	16.8	6.4	1.36	130.5	--	3.78×10^3
4	Cow Creek	13.5	1.9	0.45	84.6	--	7.25×10^2
5	Black Canyon North	5.5	1.1	0.84	24.0	3.8	6.97×10^1
6	Black Canyon South	6.2	0.5	1.09	50.0	11.2	4.03×10^1
7	Bighorn	12.1	3.7	0.55	13.3	22.7	1.13×10^3
8	Little Debbie	4.2	1.8	0.22	6.0	1.2	6.65×10^1
9	Lumpy Ridge	15.1	1.5	0.42	13.2	2.3	7.16×10^2
10	Highway 7	5.4	1.3	0.38	23.9	2.4	7.94×10^1
11	Pierson Park	7.8	4.7	3.81	54.3	8.2	5.99×10^2

In addition to the measured dimensions, an approximate failure volume for each site was estimated by calculating the volume of half an oblate ellipsoid with a vertical radius equal to the scarp height (h) and two perpendicular horizontal radii equal to the scarp width (w). Approximate failure volume (V) therefore equals:

$$V = \frac{2}{3}\pi h w^2$$

This volume is not intended to quantify the total volume of sediment movement, but rather to characterize the volume of sediment involved in the initial slope failure. To demonstrate the variability of debris flow morphology and the importance of flow bulking as the debris flow propagates downslope (Iverson et al., 2010; Frank et al., 2015), the approximate failure volume

is plotted against the maximum transport distance in Figure 4.2. Debris flows with extreme failure volumes or transport distances are labeled for discussion below. No clear relationship exists between these variables for the debris flows studied in RMNP.

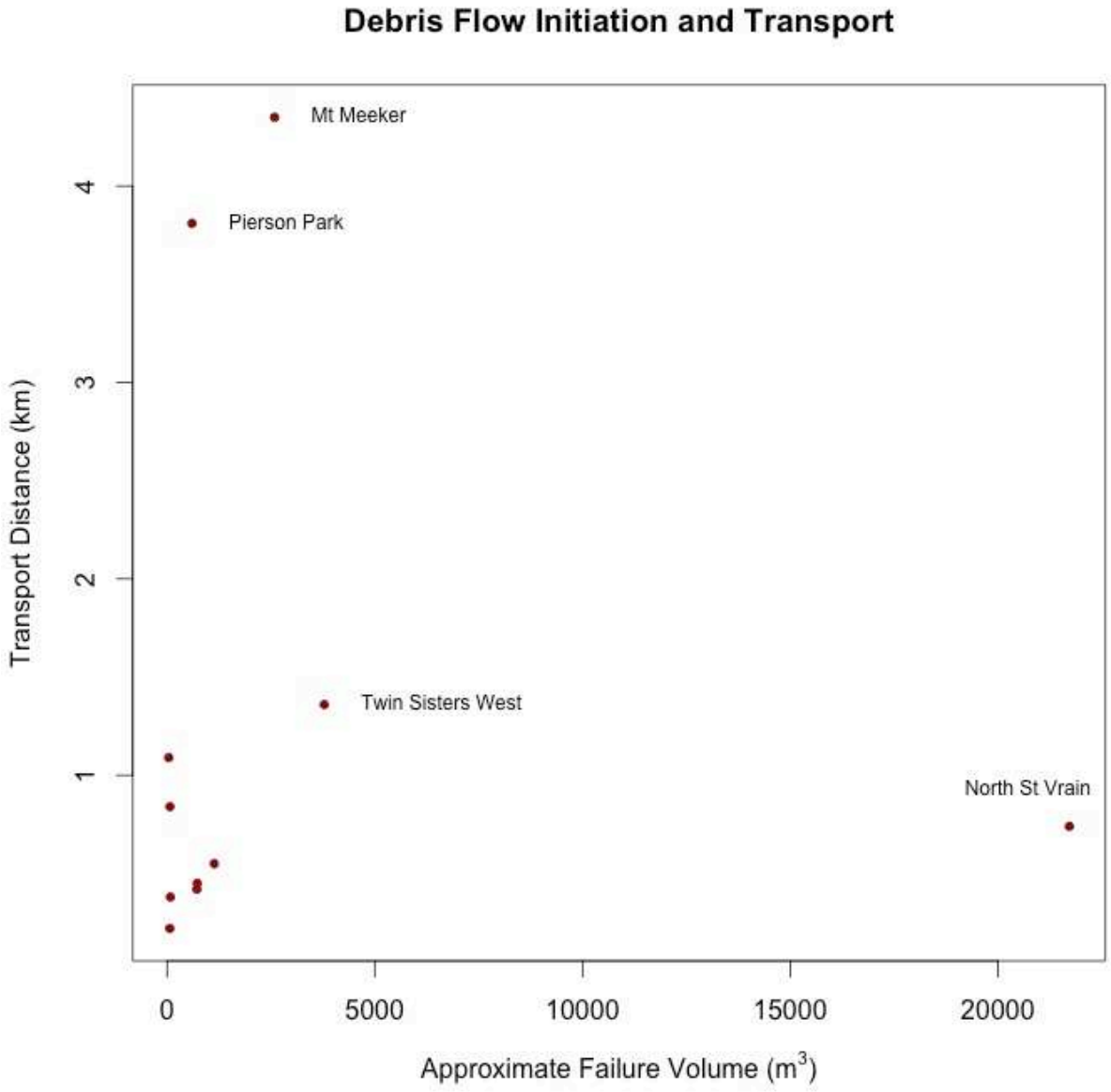

Figure 4.2. Debris flow sites plotted based on surveyed dimensions. Sites with the largest approximate failure volume or transport distance are labeled for discussion.

4.2 Site comparisons

Continuous site variables, including soil depth, contributing area, slope curvature, and soil texture (percent fines and percent organics), were compared between debris flow and control sites using two sample t-tests in most cases. Although data from the control sites did not demonstrate normal distributions in all cases, the large sample size (n = 30) in this group justifies the use of a parametric test. In these comparisons, results of the two sample t-test indicate the equality of group means by rejecting or failing to reject the null hypothesis that group means are equal (Ott and Longnecker, 2010). Where distribution of data at debris flow sites (n = 11) could not be transformed to achieve normality, a non-parametric two-sample Wilcoxon Rank-Sum test was performed to ensure that assumptions about data distribution were met. This test is commonly used as an alternative to the two-sample t-test to indicate whether the sampled populations have equal distributions by rejecting or failing to reject the null hypothesis that the ranked data distribution for both groups is equal (Ott and Longnecker, 2010). Wilcoxon Rank-Sum tests are commonly used as an alternative to two sample t-tests; although the assumptions and null hypotheses are not exactly the same, both tests indicate differences between population distributions. For both tests, a confidence of $\alpha = 0.05$ was used to determine significant difference between the sample groups. For samples where natural logarithm transformation improves the normality of the data distribution, comparative tests were performed on log-transformed data. All continuous variables were also included in an exploratory principal components analysis to assess covariate relationships and grouping of study sites. By treating debris flow occurrence as a response variable, logistic regression was also performed with all continuous variables to attempt to recover debris flow and control groups. A complete table of site data is included in Appendix A.

None of the continuous variables included in these analyses demonstrate significant differences between the study groups (see Figure 4.8-4.12 below), indicating that debris flow occurrence cannot be confidently related to specific slope variables. In complement to these findings, debris flow occurrence could not be accurately predicted using a logistic regression model that treated measured slope variables as predictors of debris flow occurrence. Despite lack of significant differences between continuous slope variables that were measured and calculated at each site, categorical field assessments of slope conditions (convergence and the presence of colluvial hollows) did demonstrate significantly different proportions at control sites and debris flow sites.

4.2.2 Control site selection criteria: Slope angle, slope aspect, and elevation

Comparison of slope data at the field-corrected control sites and debris flow sites indicated that site adjustments in the field resulted in slightly unequal distributions of slope and elevation between the two sample groups. Comparative analyses of response variables must therefore acknowledge possible confounding factors in the selection criteria. To determine whether differences in the selection criteria influenced results, t-tests were performed in conjunction with linear models that included covariates for elevation and slope angle.

Following necessary field adjustments, control sites demonstrated slightly lower average slope than the debris flow sites (Figure 4.3). Although the mean slope of these groups is not significantly different, the apparent trend may indicate that slope angle at the control sites does not reflect contitions at debris flow sites as well as intended. Slope was therefore included as a covariate in linear models for each of the response variables and in the logistic regression analysis.

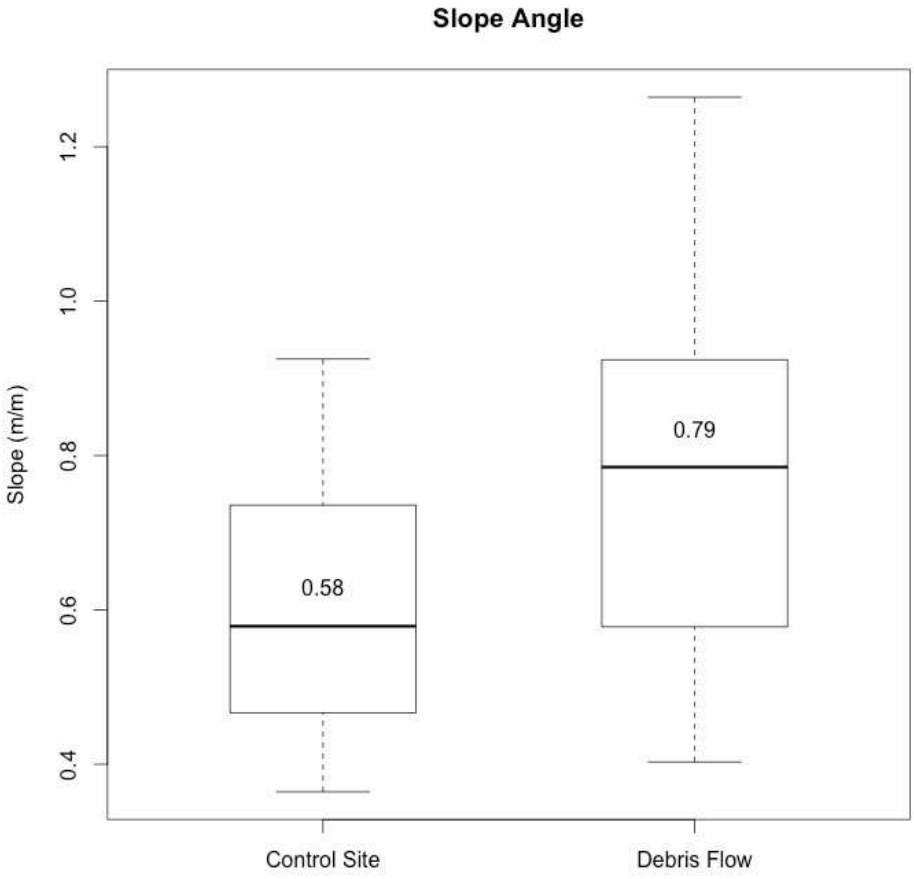

Figure 4.3. Slope angle (calculated using 10 m DEMs) at control sites and debris flow sites. The difference between group means is not significantly different. The bottom and the top of the box show the 25th ($\boldsymbol{Q_1}$) and 75th ($\boldsymbol{Q_2}$) quartiles, respectively. The lower whisker marks the larger of either the minimum value or $\boldsymbol{Q_1 - 1.5(IQR)}$ where *IQR* is the interquartile range. The upper whisker marks the smaller of either the maximum value or $\boldsymbol{Q_2 + 1.5(IQR)}$.

Field adjustments to site locations also resulted in slightly lower average elevations at control sites than at debris flow sites (Figure 4.4). Although the means of the two groups are not significantly different, the distribution and range of elevations at control sites is slightly lower than at debris flow sites. This apparent trend may indicate that elevation at the control sites does not reflect conditions at debris flow sites as well as intended. Elevation in meters was therefore

included as a covariate in linear models for each of the response variables and in the logistic regression analysis.

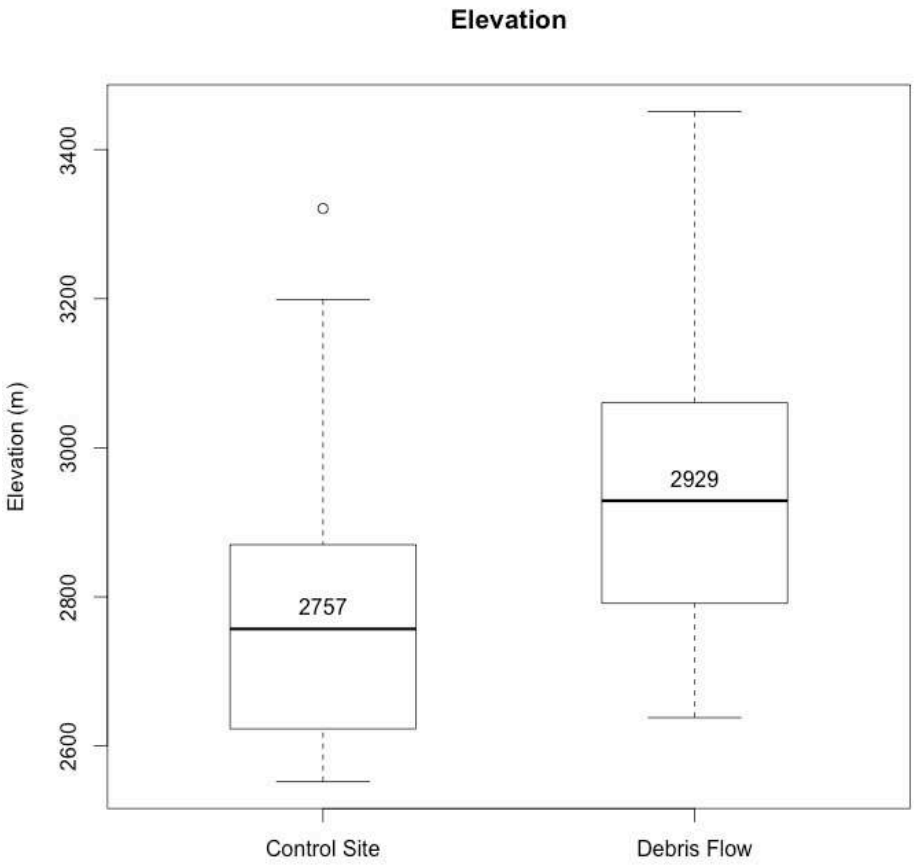

Figure 4.4. Elevation (calculated using 10 m DEMs) at control sites and debris flow sites. The bottom and the top of the box show the 25th ($\boldsymbol{Q_1}$) and 75th ($\boldsymbol{Q_2}$) quartiles, respectively. The lower whisker marks the larger of either the minimum value or $\boldsymbol{Q_1 - 1.5(IQR)}$ where *IQR* is the interquartile range. The upper whisker marks the smaller of either the maximum value or $\boldsymbol{Q_2 + 1.5(IQR)}$. Points indicate values beyond $\boldsymbol{Q_x \pm 1.5(IQR)}$.

Slope aspect was also examined at the field-corrected control sites and debris flow sites. As was intended based on the original control site selection, control sites included slopes facing all cardinal directions and no dominant aspects are apparent (Figure 4.5). Final analysis of the debris flow sites, however, indicates that most flows occurred on slopes with northeast, east, south, and

southwest aspects. Additionally, previous studies on debris flow occurrence in the Front Range (Coe et al., 2014; Anderson et al., 2015) found that debris flows initiated primarily on south- and east-facing slopes, these published findings may have been influenced by the aerial imagery available, which are primarily lit from the southwest such that north-facing slopes are shadowed and debris flows cannot be recognized as easily with remote techniques on north-facing slopes. Alternatively, the small sample size of debris flows studied in this thesis may limit resolution of patterns in slope aspect.

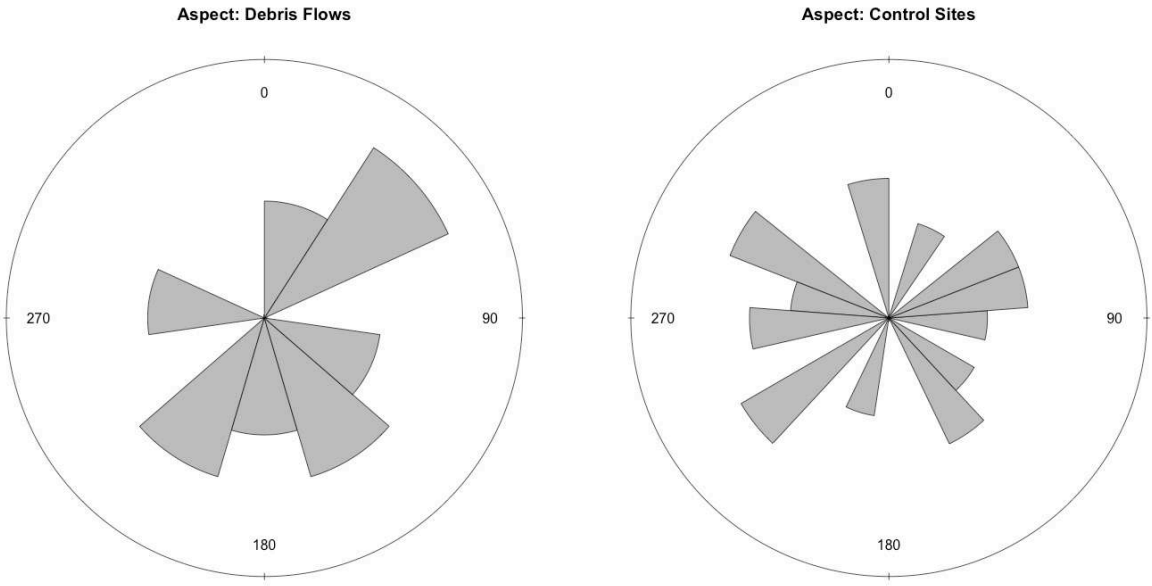

Figure 4.5. Rose diagrams showing slope aspect (azimuth) at control sites and debris flow sites. No dominant slope aspect is apparent in either group.

4.2.3 Principal components analysis

Initial data exploration included principal components analysis of the continuous variables used to compare sites (Figure 4.6). These variables include maximum measured soil depth, average soil depth, the average of the deepest three soil depth measurements, slope curvature, contributing area, percent organics in the soil and percent fines (sand/silt) in the soil. The first two principal components explain approximately 62% of the variance within the dataset. However, scores of the first two principal components cannot be used to successfully separate the control site and debris flow groups. The loadings, plotted as vectors on a biplot (Figure 4.7), indicate the magnitude and direction of influence each of these variables has on the individual scores. Related variables, such as soil depth variables and soil texture variables, plot closely together.

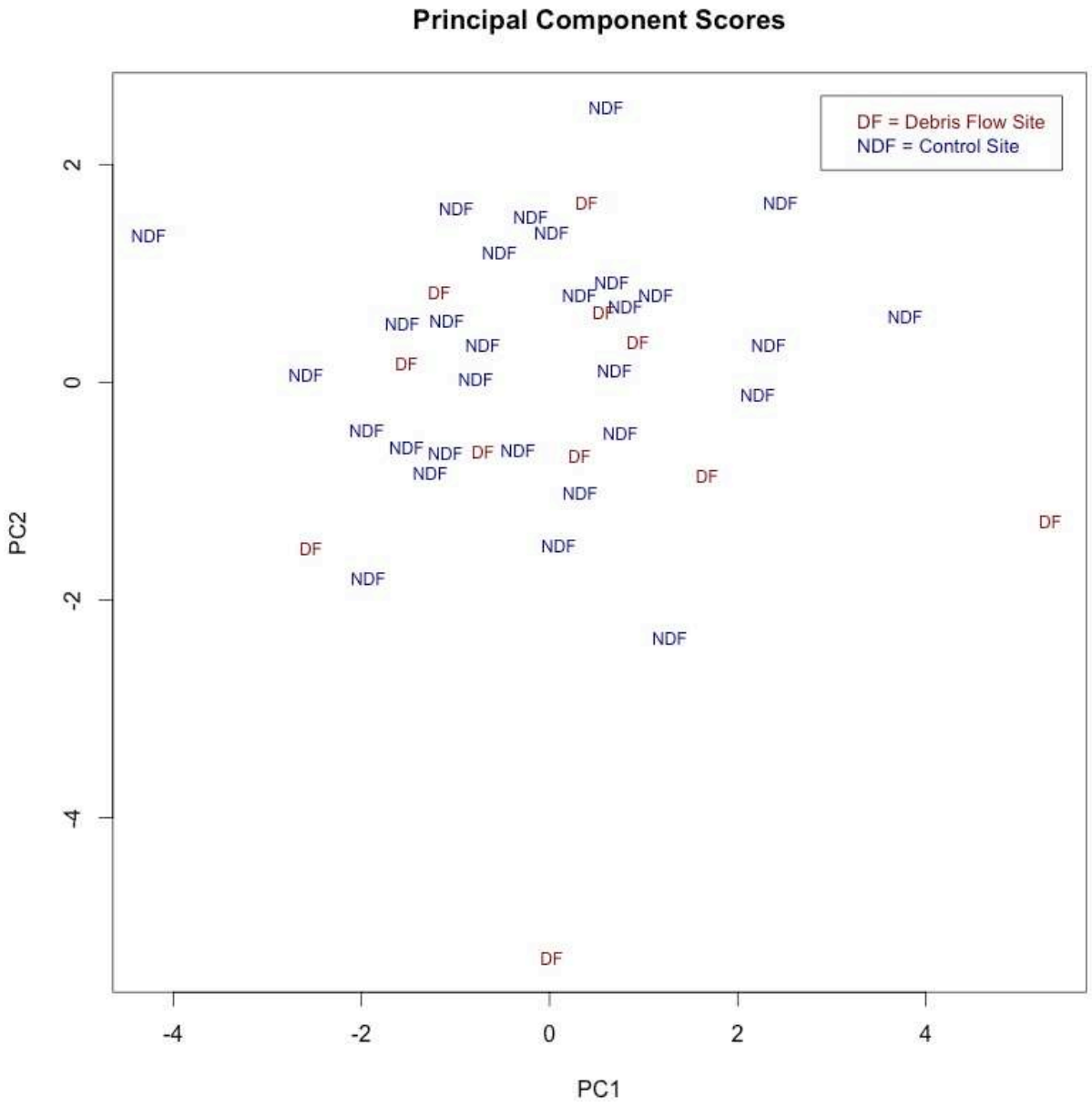

Figure 4.6. The scores of the first two principal components for both control sites and debris flow sites. The first two principal components account for 62% of the total variance, but do not successfully separate the control sites and debris flow sites.

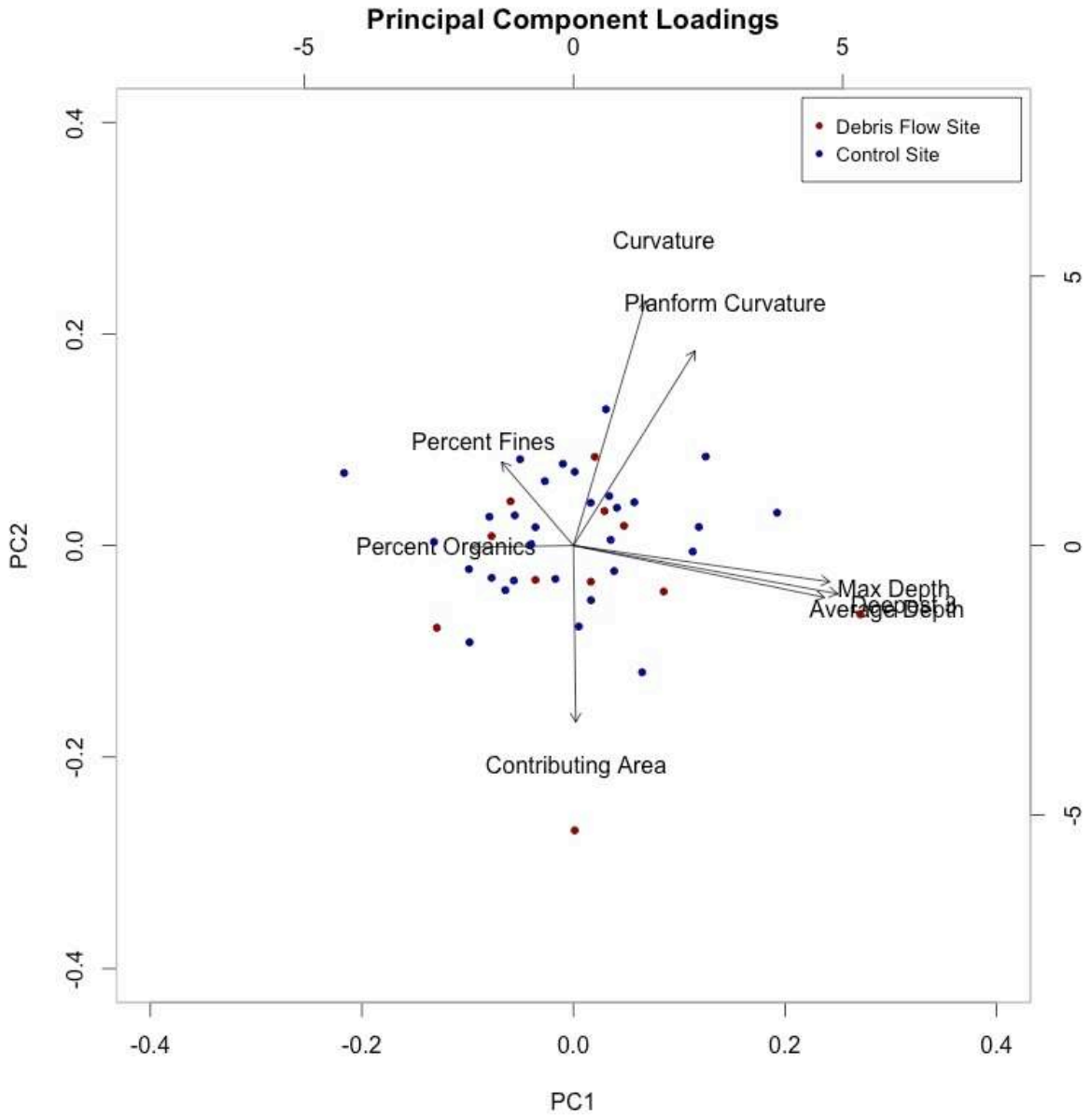

Figure 4.7. Biplot showing scores of each study site and loadings of continuous variables included in the exploratory principal components analysis.

4.2.4 Soil depth

Using the 20 soil depth measurements collected at each site, soil depth was quantified by calculating the maximum depth, the average depth, and the average of the deepest three measurements. The average of the deepest three measurements ("deepest soil depth") was used for comparative analysis, as this metric accounts for spatial variability but discards some of the shallow measurements influenced by subsurface boulders. Soil depth at control sites and debris flow sites is summarized in the boxplots below (Figure 4.8).

The mean deepest soil depth at each site is 7.3 ± 3.0 m. The deepest soil depth at debris flow sites is near-normally distributed for both sample groups. A two-sample t-test was therefore used to compare depth between these groups. Soil depth is not significantly different at control sites and debris flow sites (p-value = 0.4703).

To account for the influence of slope angle and elevation, a linear model to predict soil depth was created. Using debris flow/control site as a categorical covariate with the two selection criteria (elevation and slope angle), none of the coefficients for these variables were significant, indicating that soil depth as measured in this study is not dependent on debris flow occurrence.

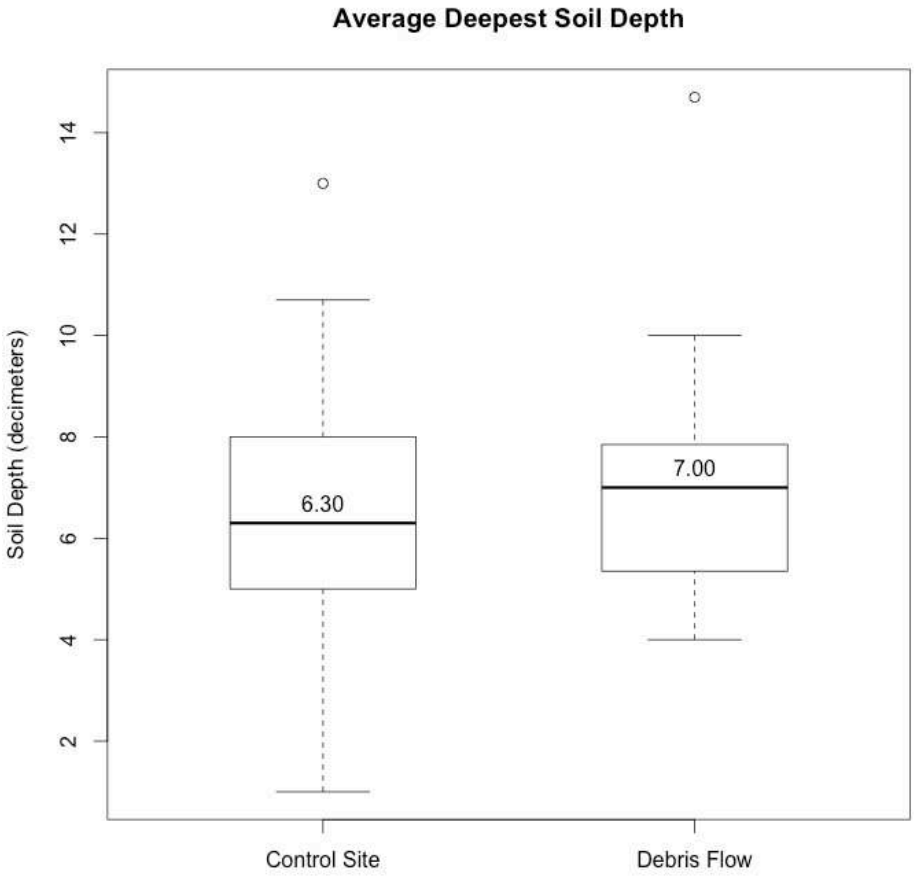

Figure 4.8. Measured soil depth at control sites and debris flow sites is not significantly different. The bottom and the top of the box show the 25th (Q_1) and 75th (Q_2) quartiles, respectively. The lower whisker marks the larger of either the minimum value or $Q_1 - 1.5(IQR)$ where *IQR* is the interquartile range. The upper whisker marks the smaller of either the maximum value or $Q_2 + 1.5(IQR)$. Points indicate values beyond $Q_x \pm 1.5(IQR)$.

4.2.5 Soil texture

At all sites, soils consisted primarily of sand and gravel. The percent sand and gravel collected from both control sites and debris flows ranged from 83-99%. Soil texture was assessed by comparing the percent fines (silt/clay) and the percent organic material extracted from soil samples, as these metrics of texture are influential in determining the hydrological properties of soils (Lohse and Dietrich, 2005). Results of textural analysis are summarized in Figure 4.9. The percent fines range from 1.83-15.1% in soils collected from control sites and 1.49-13.5% in soils

collected from hillslopes above debris flow scarps. The percent organics range from 0.01-3.48% in soils collected from control sites and 0.14-2.53% in soils collected from hillslopes above debris flow sites.

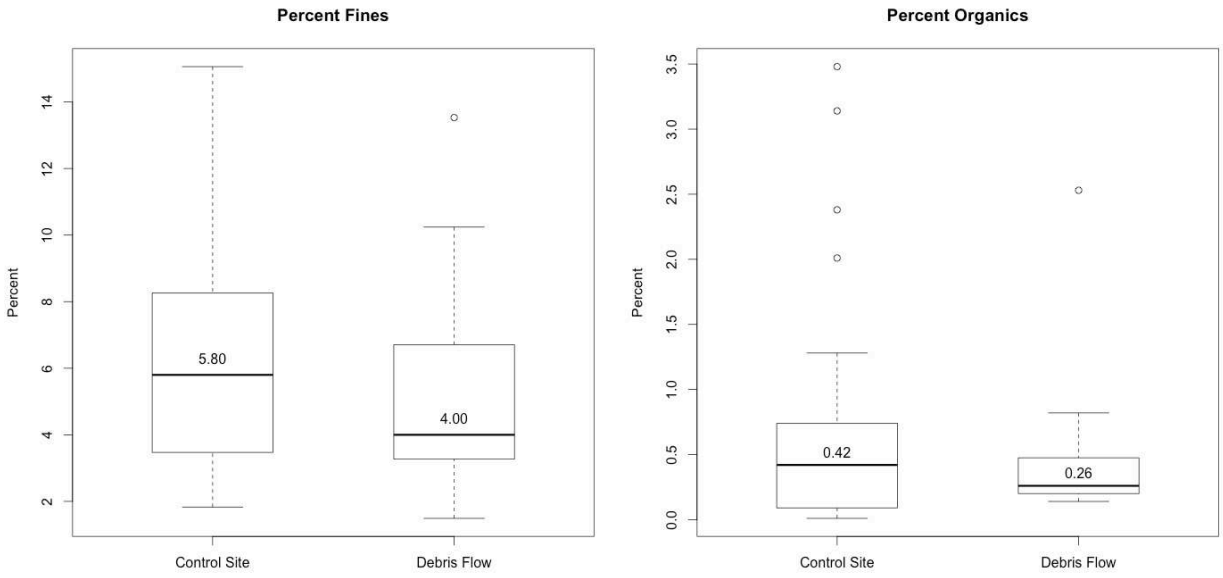

Figure 4.9. Soil texture metrics at control sites and debris flow sites are not significantly different. The bottom and the top of the box show the 25th (Q_1) and 75th (Q_2) quartiles, respectively. The lower whisker marks the larger of either the minimum value or $Q_1 - 1.5(IQR)$ where *IQR* is the interquartile range. The upper whisker marks the smaller of either the maximum value or $Q_2 + 1.5(IQR)$. Points indicate values beyond $Q_x \pm 1.5(IQR)$.

The mean percent fines at debris flow sites is 5.38 ± 3.68%. The percent fines data from both sample groups are normally distributed when log-transformed. A two-sample t-test was therefore performed on transformed data. The mean percent of fines is not significantly different at control sites and debris flow sites (p-value = 0.4187).

The mean percent organics at debris flow sites is 0.55 ± 0.70%. The percent organics data at debris flow sites could not be transformed to achieve normality. Because the sample size is not

large (n = 11), a Wilcoxon Rank-Sum test was used as a non-parametric alternative to the two-sample t-test. This test indicated that the percent organics is not significantly different at control sites and debris flow sites (p-value = 0.9531).

To account for the influence of slope angle and elevation, a linear model to predict each soil texture metric was created. Using debris flow/control site as a categorical variable and the two selection criteria (elevation and slope angle), the variable for debris flow occurrence was not significant in the model for either percent fines or percent organics, indicating that soil texture is not dependent on debris flow occurrence. The coefficient for elevation was significant in both the model for percent fines and percent organics, indicating that although soil texture does not demonstrate a clear relationship with debris flow occurrence, both soil texture metrics are correlated with elevation.

To better understand relationships between soil variables, linear regressions were created for soil depth and texture using data from all 41 study sites. The average deepest soil depth was plotted against log-transformed percent fines (Figure 4.10) and log-transformed percent organics (Figure 4.11), as log transformations generated normally distributed datasets in both cases. The transformed data do not appear to be related, either with a linear or non-linear trend. The linear models are therefore not included in the plots below. The lack of relationship is indicated by low multiple-R^2 values of regressions on soil depth vs. transformed percent fines (multiple-R^2 = 0.0779) and on soil depth vs. transformed percent organics (multiple-R^2 = 0.0250).

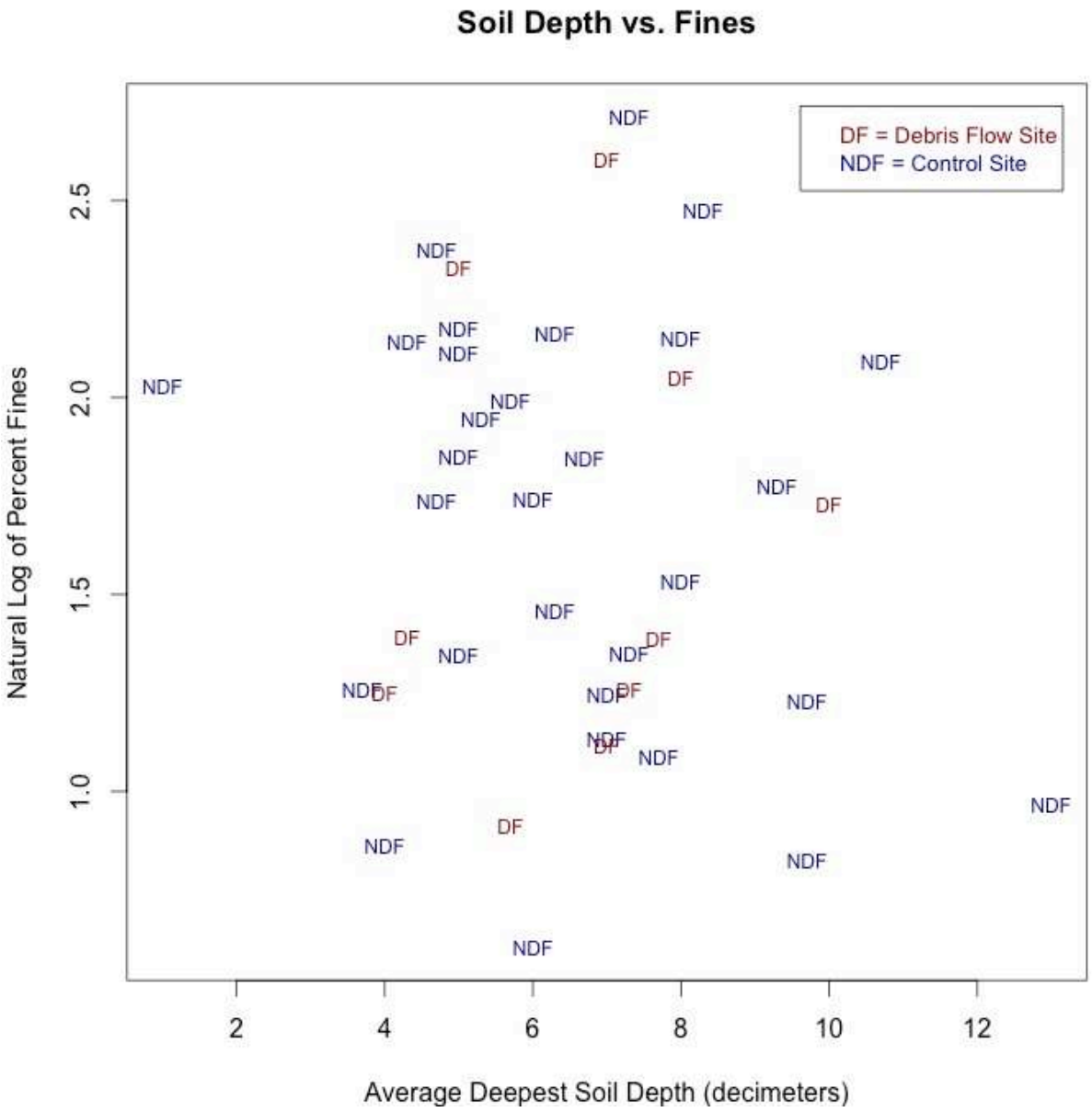

Figure 4.10. Soil depth vs. Percent fines. A linear relationship does not appear to exist between these variables. (Multiple $R^2 = 0.0779$).

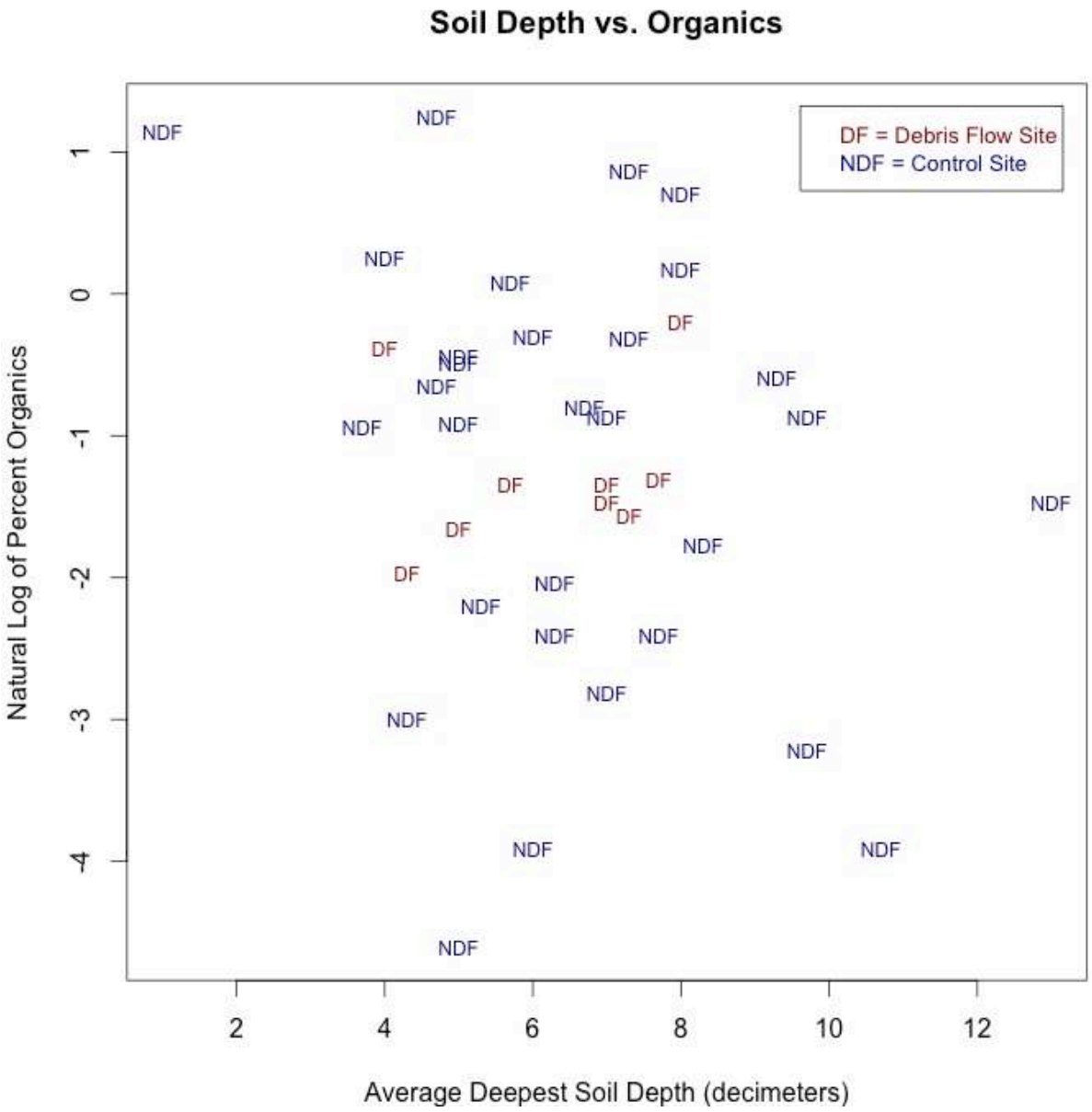

Figure 4.11. Soil depth vs. Percent organics. A linear relationship does not appear to exist between these variables. (Multiple $R^2 = 0.0250$).

4.2.6 Topography

Topographic characteristics for each study site were assessed using the contributing area and planform variables calculated from 10 m DEMs. Planform curvature (perpendicular to the slope) was the primary metric used for comparative analysis, as it better represents accumulation of groundwater and surface water flow. A negative planform curvature score indicates a slope that is concave perpendicular to the direction of maximum slope that would accumulate flow, a zero planform curvature score indicates a planar slope, and a positive planform curvature score indicates a convex slope that would generate flow divergence (Kimerling et al., 2011). Contributing area and slope curvature at both site types are compared in Figures 4.12A and B.

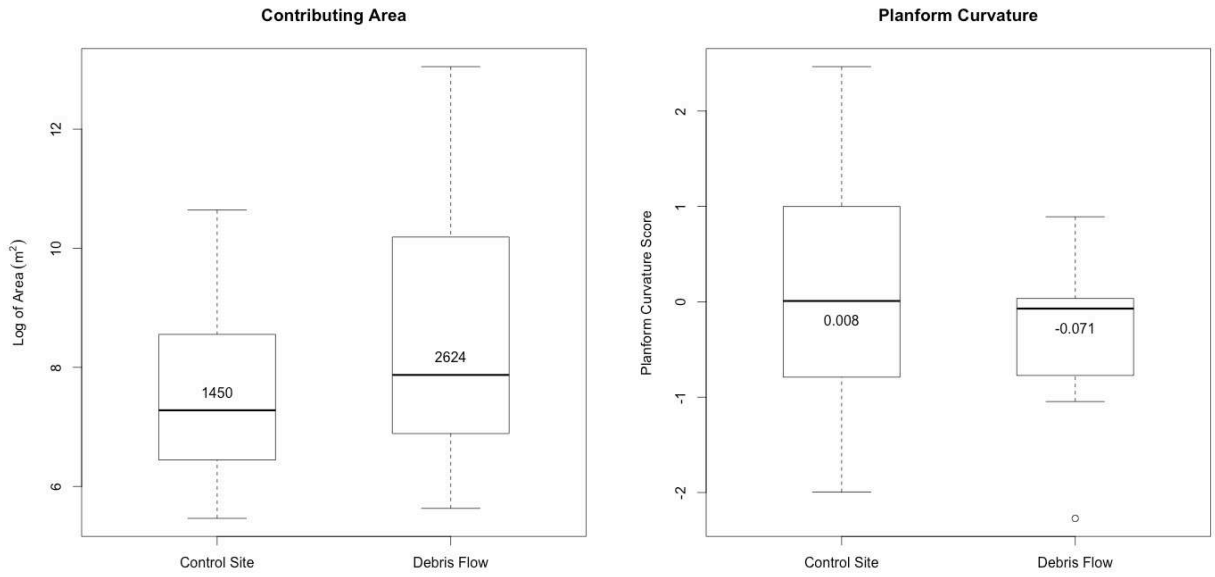

Figure 4.12A. Topographic characteristics at control sites and debris flow sites are not significantly different. The bottom and the top of the box show the 25th (Q_1) and 75th (Q_2) quartiles, respectively. The lower whisker marks the larger of either the minimum value or $Q_1 - 1.5(IQR)$ where IQR is the interquartile range. The upper whisker marks the smaller of either the maximum value or $Q_2 + 1.5(IQR)$.

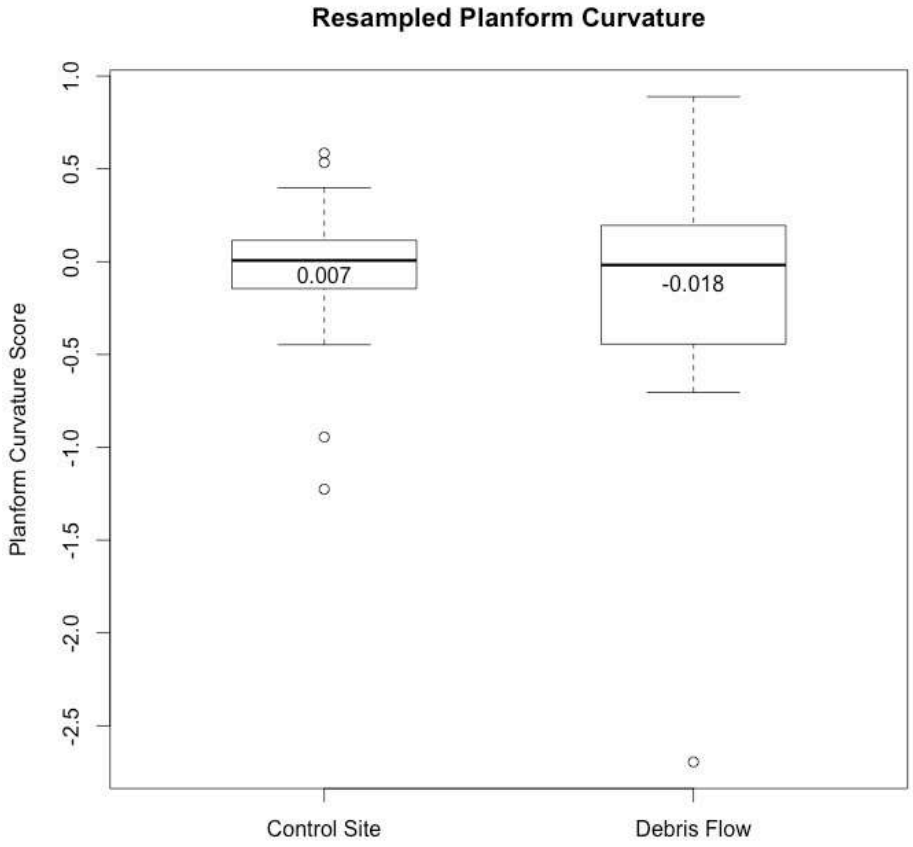

Figure 4.12B. Planform curvature scores calculated for a resampled 30 m DEM are not significantly different at control sites and debris flow sites. The bottom and the top of the box show the 25th (Q_1) and 75th (Q_2) quartiles, respectively. The lower whisker marks the larger of either the minimum value or $Q_1 - 1.5(IQR)$ where IQR is the interquartile range. The upper whisker marks the smaller of either the maximum value or $Q_2 + 1.5(IQR)$. Points indicate values beyond $Q_x \pm 1.5(IQR)$.

Mean contributing area at debris flow sites is 53,017 ± 137,540 m^2. Contributing area is distributed approximately normally at both debris flow and control sites when the datasets are log-transformed. A two-sample t-test was therefore used on transformed data to test for difference of the group means. The mean contributing area is not significantly different at control sites and debris flow sites (p-value = 0.145).

Mean planform curvature at debris flow sites is -0.35 ± 0.83. Planform curvature data calculated using a 10 m DEM could not be transformed to achieve normality in both groups. Because the sample size of debris flows (n = 11) is not large, a non-parametric two-sample Wilcoxon Rank-Sum test was used to test for difference of the group means. The mean planform curvature score was not significantly different at control sites and debris flow sites (p-value = 0.251).

Mean resampled planform curvature at debris flow sites is -0.10 ± 0.57. Resampled planform curvature data calculated using a 30 m DEM are distributed normally at both debris flow and control sites. A two-sample t-test was therefore used on the raw data to test for difference in group means. The mean resampled planform curvature is not significantly different at control sites and debris flow sites (p-value = 0.482).

To account for the influence of slope angle and elevation, linear models to predict topographic characteristics were created. Using debris flow/control site as a categorical variable and the two selection criteria (elevation and slope angle), the variable for debris flow occurrence was not significant in the model for either contributing area or planform curvature, indicating that topography is not dependent on debris flow occurrence.

In addition to comparison of continuous slope variables, proportions of field classifications were also compared between study groups. Field assessments of each site included classification of whether the site was located in or directly below a colluvial hollow and whether each site was located in an area of convergent topography. Sites classified as having “convergent topography” included areas near colluvial hollows as well as areas of broader slope convergence. Results of

these classifications are summarized in Table 4.2, along with significance indicated by a two-sample test for equality of proportions. Debris flow sites showed significantly higher proportions of both colluvial hollows and generally convergent topography.

Table 4.2. Field classifications of site topography. Significantly different proportions are indicated by bold lettering.

	Colluvial Hollow	No Colluvial Hollow	Total	Proportion with Hollow	Significance
Debris Flows	4	7	11	0.36	**p-value = 0.0201**
Control Sites	1	29	30	0.03	

	Convergent Topography	No Convergence	Total	Proportion Convergent	Significance
Debris Flows	8	3	11	0.73	**p-value = 0.0003**
Control Sites	3	27	30	0.10	

4.2.7 Vegetation

All three vegetation classes (coniferous forest, brush, and herbaceous plants/grasses) were observed in the field at both debris flows and control sites, with the exception that no debris flow sites were classified as having primarily herbaceous vegetation (Table 4.3). Because the sample size was small (some combinations of vegetation and site type had few or zero counts), Fisher's Exact Test was used to test the dependency of vegetation type and debris flow occurrence on each other. This test failed to reject the null hypothesis that the categorical variables (vegetation and site type) are independent. Debris flow occurrence cannot be conclusively related to dominant vegetation type at the study sites.

Table 4.3. Field classifications of dominant vegetation type at each site. The vegetation categories and debris flow occurrence were not significantly dependent upon each other.

	Coniferous	Brush	Herbaceous	Total	Significance
Debris Flows	4	7	0	11	p-value = 0.2071
Control Sites	18	10	2	30	

4.2.8 Fire history

Only one of the 11 debris flow sites occurred in an area that has experienced documented wildfire within the past 60 years; the failure location of the North St. Vrain debris flow occurred within the area of the 1978 Ouzel Fire. This site was characterized by broadly convergent topography, and therefore did not deviate from patterns in geomorphic conditions observed at other debris flow sites in RMNP. None of the control sites were located in areas of recent fire.

4.2.9 Predicting debris flow occurrence

By treating the site type (debris flow or control site) as a binary response variable, all continuous covariates discussed above can be treated as possible predictors of debris flow occurrence. Predictions were created using two binary classification techniques that fit models to 35 randomized training observations (~85% of the 41 total observations). Debris flow occurrence was treated as a factor such that a response = 1 indicated a debris flow site and response = 0 indicated a control site. All continuous site characteristics (aspect, slope, soil depth, percent fines in the soil, percent organics in the soil, contributing area, and planform curvature) were input as possible predictor covariates.

Due to the large number of covariates relative to the number of observations, the data are linearly separated such that standard logistic regression cannot be performed. Logistic lasso regression was therefore used as a regularized alternative. Logistic lasso returned a model with one non-zero coefficient for contributing area.

$$Debris\ flow\ occurrence = 1.274e^{-5} \times contributing\ area$$

This model indicates that contributing area is the best predictor of debris flow occurrence. When applied to the complementary training data set, the model correctly predicted 4 of 6 observations (67%) as control sites with no debris flow occurrence. The low value of the coefficient for contributing area in this model indicates that it will only predict debris flow occurrence in the case of very large drainages, and predicts no debris flow occurrence in most cases. After this model was identified, a second logistic lasso model was used to reduce the bias introduced by one debris flow site with a very large contributing area (the North St. Vrain site). This second model excluded the North St. Vrain site and returned nonzero coefficients for both slope and contributing area. However, both coefficients were very small (10^{-2} and 10^{-5}, respectively) and the model predicted no debris flow occurrence for all six test cases.

In addition to logistic lasso regression, continuous covariates were also used to predict debris flow occurrence using linear discriminant analysis (LDA) to separate site types with linear boundaries. LDA was generated using the same training and test sets used for lasso regression analysis. This technique accurately predicted 4 of 6 observations, including 1 of 2 debris flows (50%) and 3 of 4 control sites (75%).

4.3 Debris flow chronology

Numeric and relative ages of the older debris flow deposits, including the old debris flow fan that underlies the Bighorn Ranger Station and old debris flow levees, indicate that at least 2-3 older debris flows have occurred at this site in the last 10^2-10^3 years. This interpretation is based on preservation of two old debris deposits in the fan and segments of three old debris flow levees. Two of the debris levees may have been deposited as the levees of a single debris flow or in

separate flows. Results of the numeric and relative geochronologic techniques are described individually in the sections below and summarized in section 4.3.8.

4.3.1 Deposit mapping

Pictures of the mapped debris flow levees are shown in Figure 4.13. The 2013 debris flow deposits and older deposits are shown in the map of the Bighorn debris flow site (Figure 4.14). Assuming that a debris flow effectively entrains any older debris deposits in its path, the outermost levee deposits are necessarily older than those closer to the primary 2013 debris flow channel. Based on field relationships, Levee 3 must be the oldest deposit and Levee 1 is the youngest deposit excepting the 2013 deposits.

In addition to mapped levee locations, observations of greater diffusion and surficial weathering of Levee 3 relative to Levees 1 and 2 further indicate that Levee 3 is older than the two levees closer to the 2013 deposit.

A. B.

Figure 4.13. A: Photo showing the crests of Levee 1 and Levee 2, which were both characterized by sufficient topographic relief to be elevated above the surrounding terrain. B: Photo showing alignment of boulders in Levee 3, which exhibited a much more subdued topography.

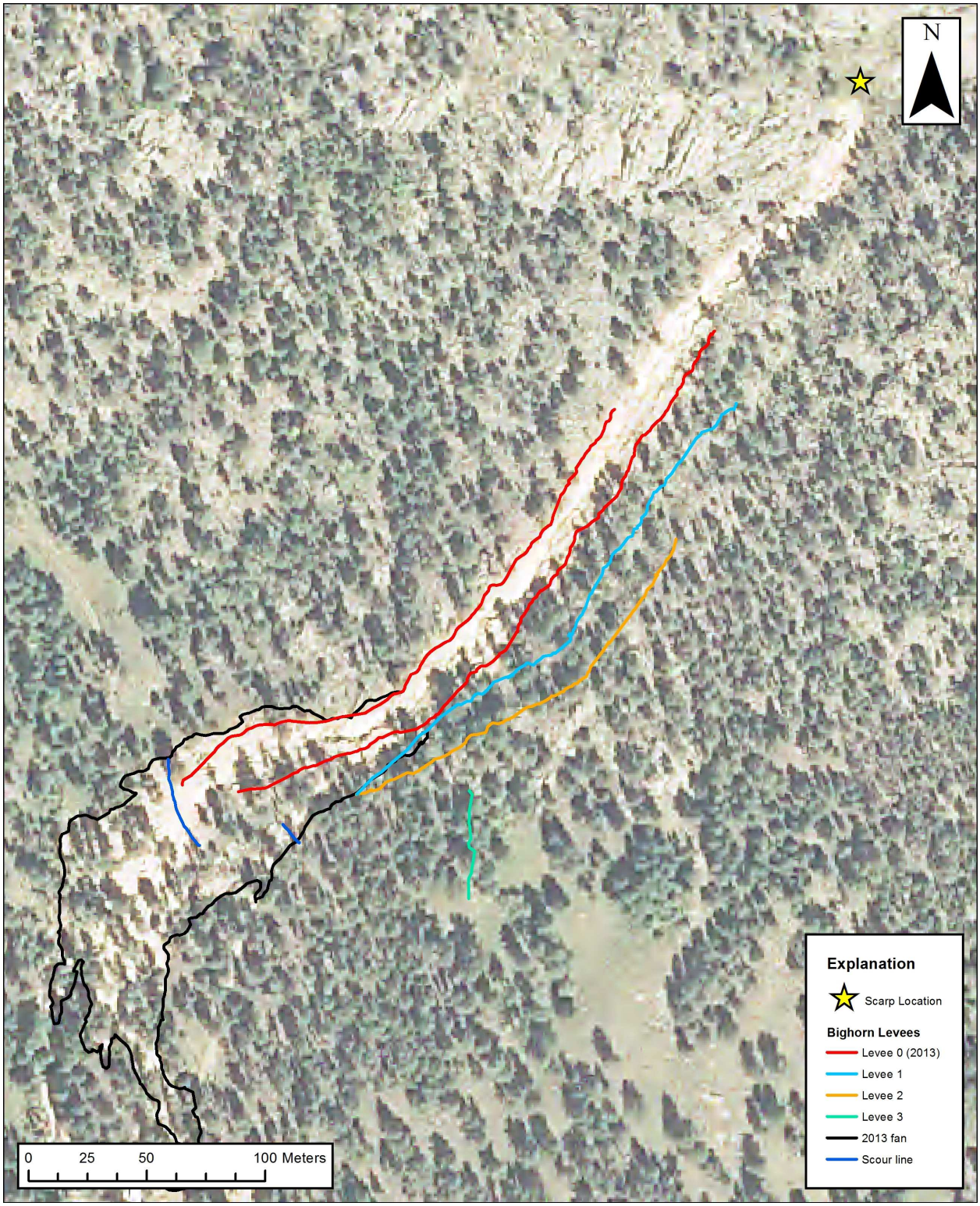

Figure 4.14. Map of the 2013 debris fan at the Bighorn debris flow site, the 2013 debris flow levees, and older debris flow levee deposits.

4.3.2 Stratigraphy

Excavation of a 4 m long, 1 m deep trench in the distal portions of the Bighorn debris fan exposed old debris flow sediments below developed soil horizons (Figure 4.15).

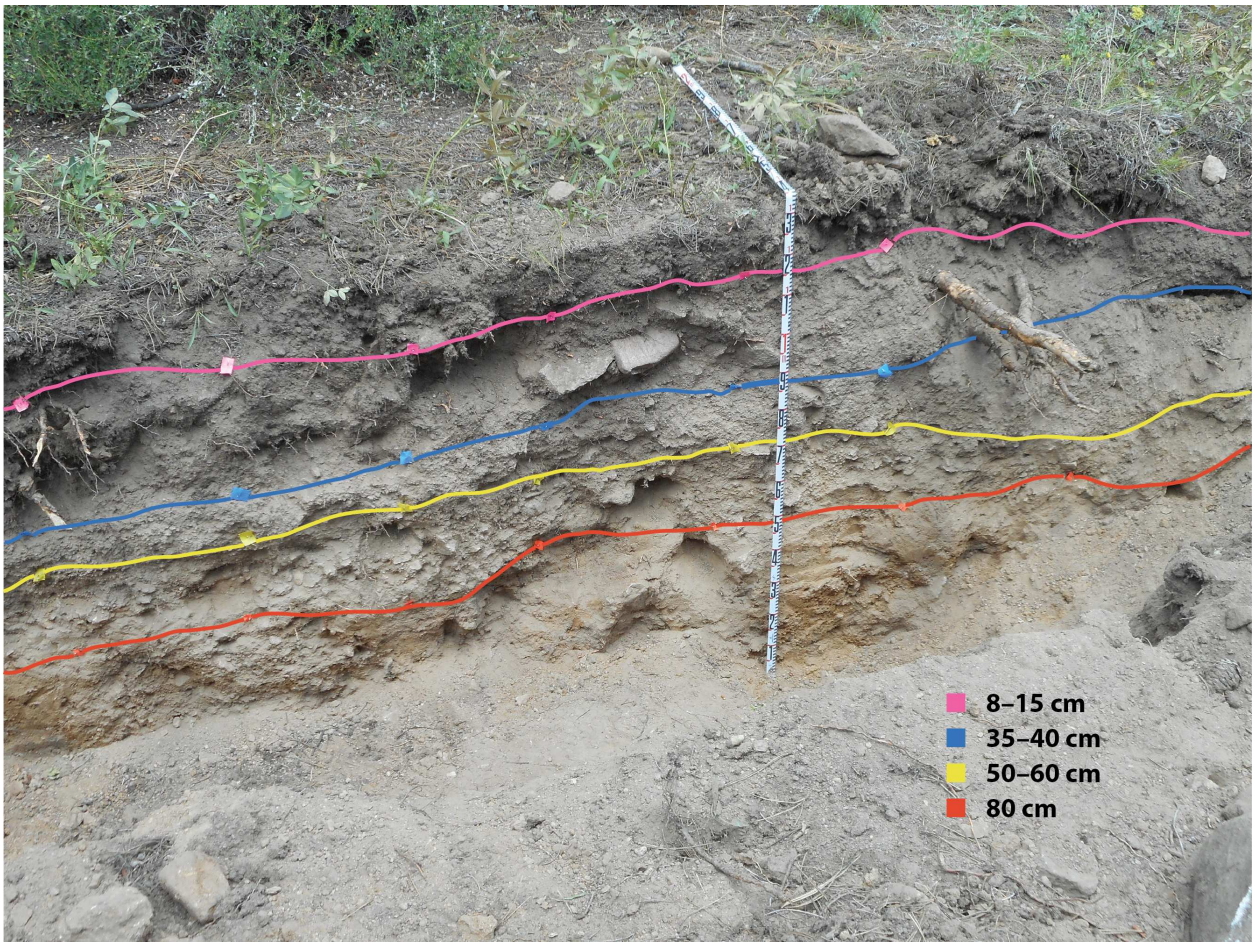

Figure 4.15. Trench stratigraphy; deposits are separated by colored flags. Annotations delineate stratigraphic layers described below, labeled with approximate depth from the surface. Organic material (Sample 9) was collected from the lower debris deposit for radiocarbon analysis.

An organic-rich A horizon was exposed between 0 and 8-15 cm depth (above the pink flags in Figure 4.15), underlain by sandy soil between 8 and 35-40 cm (above the blue flags). Exposed from approximately 35 to 50-60 cm depth was a dense, poorly sorted, pebbly sand layer (above the yellow flags). This pebbly sand is underlain by an unsorted, dense, angular, matrix-supported

gravel from 50-80 cm depth (above the orange flags). Below 80 cm depth, a very dense, partially oxidized, angular, clast-supported gravel was exposed (below the orange flags). The deposits exposed below soil horizons were interpreted as a hyper-concentrated flow deposit overlying two old debris deposits. One sample of organic material was collected from the trench near the bottom of the exposure and was analyzed for radiocarbon age as described below.

4.3.3 Radiocarbon analysis

Ages returned from selected carbon samples are summarized in Table 4.4. Ages were corrected for isotopic fractionation by DirectAMS and reported in years before present (BP), or years before 1950. None of these ages correspond to other ages established through any of the geochronologic techniques in this study.

Table 4.4. Radiocarbon ages of samples collected at the Bighorn debris flow site. The quality of the sample was determined based on field observations that indicate the relative ability of each sample to accurately date the debris deposit. These ^{14}C ages are summarized with other numeric and relative dating techniques in section 4.3.8.

Sample	Age (yrs BP)	Error	Collection Notes	Quality
1	585	27	From exposure in debris channel	Good
4	Modern	--	From exposure in debris channel	Fair
5	337	23	Wood pinned between boulders on levee 1	Excellent
6	920	31	From exposure in debris channel	Fair
8	46	21	Wood pinned between boulders on levee 2	Good
9	405	29	Collected from the excavated trench	Fair

4.3.4 Aerial photos

Due to low resolution of the available aerial photos, old debris flows could not be positively identified on aerial imagery created before 2013.

4.3.5 Lichenometry

Lichen diameters of three species were compared between Levees 1 and 2 (Figure 4.14 above). The three species chosen for study at this site were distinguished as the green, brown, and gray species. Boxplots showing measured colony diameters are shown in Figure 4.15, colored by levee. Two-sample t-tests for significantly different means were run, as sample sizes were large in all cases (141-154 lichens of each species were measured on each levee). A standard $\alpha = 0.05$ confidence was used to determine significantly different means between levees. The relative ages indicated by lichen diameters corroborate relative ages established by spatial relationships and field observations.

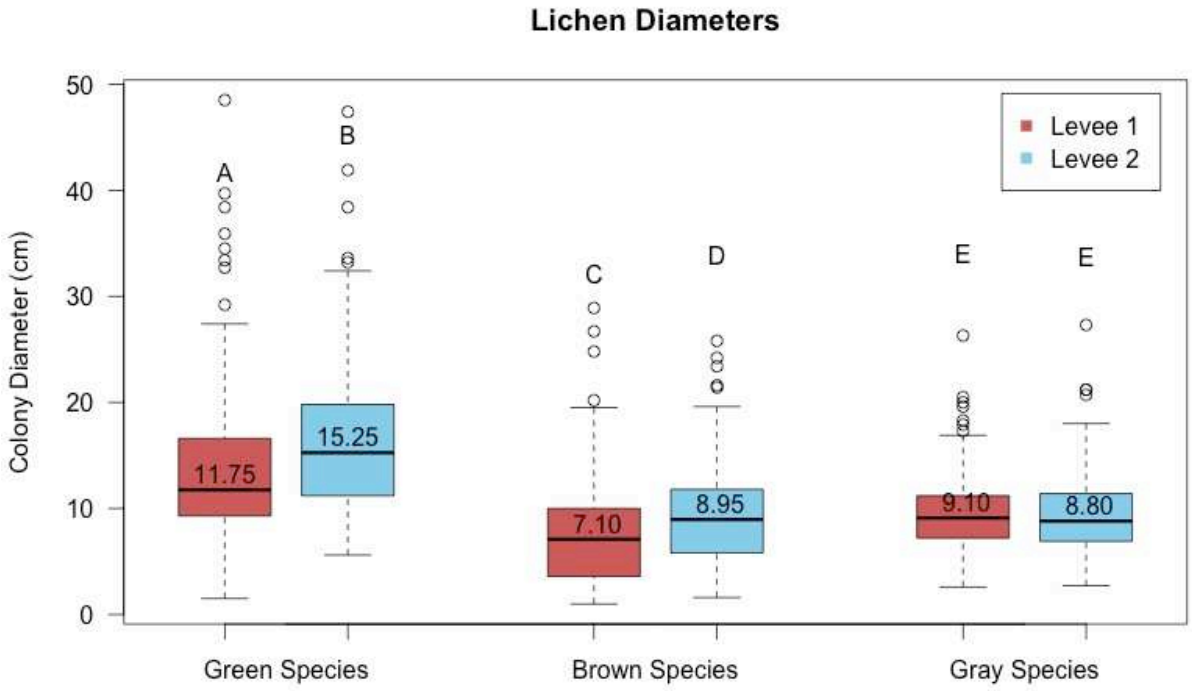

Figure 4.15. Lichen colony diameters measured on levees 1 and 2. Letters indicate statistical difference (e.g., A, B) or similarity (e.g., E, E) of lichen diameters on the two levees.

The green and brown lichen species demonstrated significantly different colony diameters on levees 1 and 2 (p-value = 0.0015 and p-value = 0.0021), respectively. In both cases, the larger lichens were observed on levee 2. The gray lichen species did not demonstrate significantly different colony diameters on levees 1 and 2 (p-value = 0.6158).

4.3.6 Dendrochronology

One tree wedge was collected for dendrochronologic analysis. Photos of the sample wedge are shown in Figure 4.16. As indicated by the number of incomplete rings that have grown outside of the scar tissue, the age of scarring is approximately 172 years before 2013. This age was achieved by counting growth rings from the outside towards the scar tissue, with multiple points along the circumference of the wedge yielding the same age.

Figure 4.16. Tree wedge studied for dating of the scar. Blue lines mark every tenth growth ring.

4.3.7 ^{10}Be radionuclide analysis

Radionuclide analysis of boulder samples collected from the Bighorn debris flow levees returned exposure ages that ranged from 7.97 – 196 ka. Exposure ages are listed and summarized in the boxplot (Figure 4.17). 'Levee 0' indicates samples collected from the 2013 debris flow levee. Samples collected from levees 1, 2, and 3 are from the older levees shown in the deposit map above (Figure 4.14).

Table 4.5. ^{10}Be exposure ages collected from debris flow levees at the Bighorn site. These exposure ages are summarized with other numeric and relative dating techniques in section 4.3.8.

Sample	Levee	Exposure Age	Internal uncertainty
1	2	55,525	4,940
3	2	46,960	4,178
4	2	14,107	1,268
5	2	7,966	802
6	2	45,570	4,062
7	1	84,502	7,564
8	1	70,232	6,396
9	1	30,288	2,707
10	1	47,113	4,200
11	0	18,068	1,602
12	3	74,562	6,658
13	3	196,034	17,977
14	3	103,166	9,315
15	2	151,897	13,810

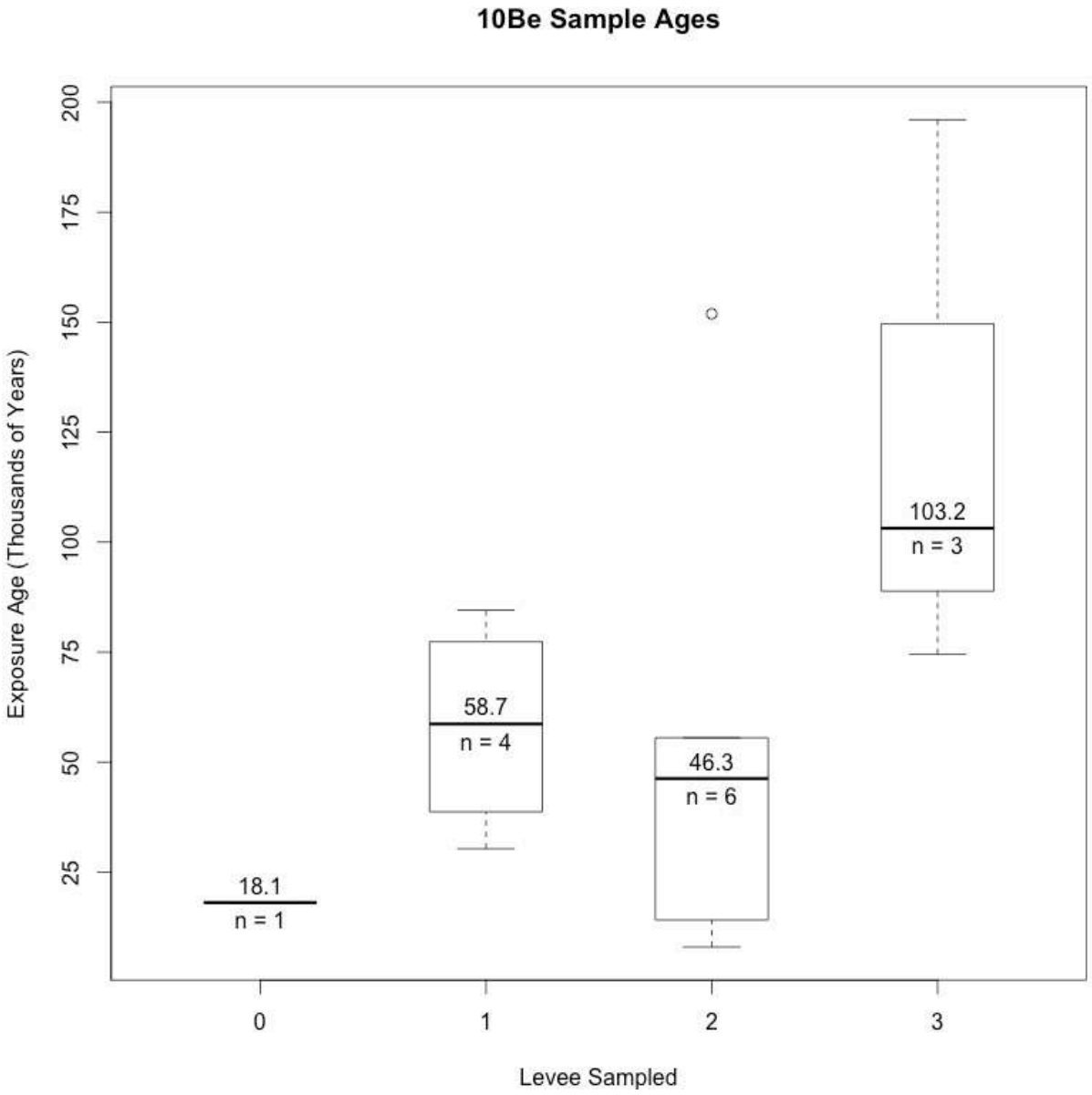

Figure 4.17. Exposure ages calculated for samples collected from the 2013 and older debris flow levees using cosmogenic ^{10}Be concentrations. The mean exposure age of samples collected from each levee is not significantly different from the mean exposure ages of the other levees.

Because of the large range of ages calculated for samples from each levee, and because the sample collected from the 2013 levee returned a non-zero exposure age, these ages do not appear to accurately reflect the time since the mass movements that deposited the sediment. Instead, the

sampled boulders must demonstrate older ages due to inheritance of ^{10}Be accumulation before the mass movements occurred. Inherited exposure age may result from exposure of the sampled rock on the cliff face above the scarp or from storage in the colluvial hollow prior to each event. Furthermore, inheritance of exposure age indicates that transport in the debris flow did not erode sufficient surface material from the sampled boulders to "re-set" the exposure time. The exposure history of each particle sampled therefore reflects a unique history of downslope transport and residence in temporary sinks such as the colluvial hollow or cliff exposure. Although the ages of boulders from each levee do not significantly differ, it does appear that boulders collected from Levee 3 have been exposed to the atmosphere longer than boulders in Levees 1 and 2, which corroborates the relative age of these levees determined from spatial relationships. Assuming that calculated ages do not indicate falsely young exposure ages, the youngest boulder sample collected from each levee is the maximum age of the levee. These exposure ages therefore indicate that levees 1, 2, and 3 are no older than 30 ka, 8 ka, and 75 ka, respectively. Based on field relationships and the differences in lichen colony diameters, it is likely that levee 2 is older than levee 1 and that both levees are therefore younger than 8-14 ka.

4.3.8 Compilation of numeric ages

All numeric ages determined for deposits at the Bighorn debris flow site are summarized in Figure 4.18, along with locations of the old debris flow levees shown above (Figure 4.17). As described above, Levee 3 is interpreted as the oldest of the old debris flow deposits based on spatial relationships, field observations, and apparent clustering of median ^{10}Be exposure ages. Levees 1 and 2 are older than the 2013 deposit but younger than Levee 3 and may have formed in the same or separate events.

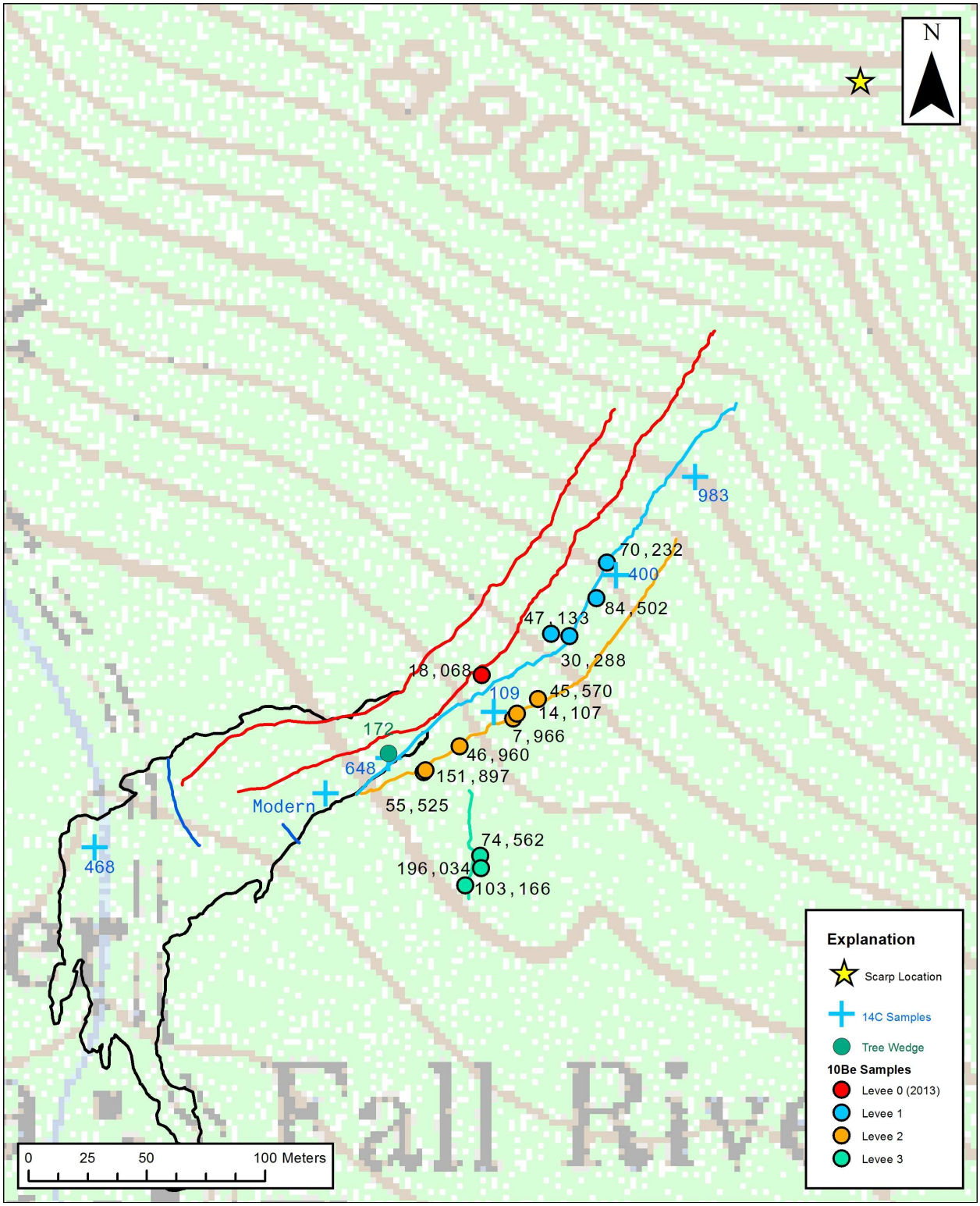

Figure 4.18. Map of numeric ages of samples collected from the Bighorn debris flow site as determined by all geochronologic techniques described above. For ease of comparison between methods, ^{14}C years BP have been converted to radiocarbon years before 2013.

5. DISCUSSION

5.1 Debris flow surveys

The debris flows surveyed in this study exhibited highly variable morphologies. The metrics used to characterize channel and deposit morphology, including transport distance and approximate failure volume, are not consistent between sites. Furthermore, the lack of correlation between approximate failure volume and maximum transport distance indicates that other factors, such as bulking along the flow path or the composition of the flow, are primarily responsible for the distance of sediment transport. Thus, the total volume of sediment eroded and transported along the length of the debris flow channel is more dependent on bulking than on the size of the initial failure. These findings are consistent with previous studies that highlight the importance of in-channel processes rather than failure magnitude in determining the volume and transport distance of debris flows (Costa, 1984; Iverson, 1997; Iverson et al., 2010; Iverson, 2014; Frank et al., 2015).

Two debris flows transported material unusually long distances (Pierson Park and Mt. Meeker) despite having initiated with moderate or low failure volumes. In addition to the large volume of material available to be eroded along the debris flow channel, both of these flows occurred on hillslopes with ample space for debris flow propagation; neither slope shallowed into a low-angle valley for several kilometers. Conversely, one debris flow site (North St. Vrain) had an unusually large approximate failure volume but a short transport distance. The North St. Vrain debris flow initiated next to a small stream that appears to have removed lateral support during the 2013 storm and allowed for a very large failure scarp. The total transport distance, however, is relatively short, as this debris flow entered the low-gradient North St. Vrain river valley in 0.74

km with a nearly perpendicular entry angle. Convergence with the stream at this high angle would have effectively halted the flow, as debris flows that enter a pre-existing stream channel at angles >45° are more likely to end at the stream than those that enter stream channels at a smaller angle (Guthrie et al., 2010). These sites with extreme transport distance or failure volume demonstrate most clearly the influence of downslope bulking and downslope topography (Guthrie et al., 2010) on total transport distance.

The majority of the debris flow channels surveyed were contained between well-defined levees. Only two debris flows (Twin Sisters West and the Cow Creek) were characterized by broad, unconfined deposits along much of their flow paths, similar to the "open" debris flow morphology described in Guthrie et al. (2010). These two flows were likely more fluidized than the channelized flows in RMNP. It is unclear what variables may have resulted in this morphologic dichotomy, but possible controlling factors on debris flow width (and, by proxy, debris flow confinement) include slope angle (Guthrie et al., 2010), grain size distribution (Whipple and Dunne, 1992; de Haas et al., 2015), bulk-sediment concentration (Whipple and Dunne, 1992), and the presence or absence of confining topography downslope of the scarp. Observed groundwater flowing from the base of the Twin Sisters West failure scarp indicates that a groundwater component influenced the low viscosity (low sediment concentration) nature of this debris flow and, in concert with the divergent topography downslope of the scarp, resulted in the wide, unchannelized morphology of this debris flow.

5.2 Site Comparisons

Most of the metrics used to characterize hillslopes in RMNP could not be used to distinguish debris flow sites and control sites. With the exception of field assessments of slope morphology, slope variables could not be significantly separated according to site type and could not accurately predict debris flow occurrence. Slope variables (excepting categorized slope morphology) were not significantly different at debris flow sites and control sites, and neither logistic regression techniques nor principal components analysis successfully separated site types. These results indicate that most of the variables measured, including soil depth, contributing area, soil texture, and continuous slope morphology metrics cannot be used as reliable predictors of debris flow hazard in RMNP.

Only two of the variables measured in this study demonstrated significant differences between debris flow and control sites. Field assessments of convergent topography and the presence of a colluvial hollow indicate that these characteristics do occur more frequently at debris flow sites. This distinction indicates that slope morphology is an important control on debris flow initiation, and Hypothesis 1 is therefore partially substantiated.

The lack of significant difference between the other measured slope variables (soil depth, soil texture, calculated topographic metrics, etc.) at debris flow sites and control sites and the limited predictive value of these variables on debris flow occurrence could result from a number of possible influences. The lack of correlation between these variables and debris flow occurrence may indicate that the measured variables are not causally linked to debris flow initiation; that field measurements did not accurately describe slope characteristics that are important

controlling variables; that sample size limited the power to discern differences between sites; and/or that debris flow occurrence results from a complex interaction of slope conditions that could not be fully captured in a study of this scale. It is likely that general lack of substantive findings in this study reflects a combination of these possibilities. For example, this study did not assess localized variations in cumulative precipitation and short-interval rainfall intensity, underlying lithology, or joint spacing, factors that may have confounded geomorphic conditions at each site. Furthermore, the sample size of debris flow sites (n = 11) is not large and may limit the descriptive power of geomorphic characterization of debris flows in RMNP. Specific data limitations and interpretations of potentially unrecognized geomorphic control are discussed in the sections below.

5.2.1 Soil depth

Comparison of soil depth at debris flow sites and control sites was hindered by the reliability of field measurements. Hillslope soils throughout the study region are developed in colluvium and glacial deposits from the Pinedale (late Pleistocene) and Bull Lake (middle Pleistocene) glaciations (Braddock and Cole, 1990; Madole et al., 1998), and as such are very rocky, with large cobbles and boulders common at all study sites in RMNP. Rocky soils limited the accuracy of mechanical soil depth measurements; measured soil depth at debris flow sites was consistently lower than the observed height of exposures of unconsolidated material in debris flow scarps. Based on these observations, depth to refusal of the soil probe likely does not indicate total soil depth, but rather the depth at which the probe encountered a large cobble or boulder. To more accurately characterize soil depth at these sites would require use of geophysical techniques, such as ground penetrating radar or electrical resistivity.

Despite the inconclusive nature of soil depth comparisons in this study, availability of source material is an important controlling variable on debris flow occurrence (Lumb, 1975; Costa, 1984; Anderson et al., 2015). By proxy, an accurate measure of soil depth should be a valuable metric in determining a slope's susceptibility to failure. It is therefore likely that the lack of significant difference in soil depth found in this study reflects the difficulty in accurately measuring soil depth rather a lack of control on debris flow initiation.

5.2.2 Soil texture

Soils collected from all study sites in RMNP demonstrated minimal variability in soil texture. All samples contained a high proportion of sand and gravel (83-99%) a small proportion of finer material (1-15%), and a small proportion of organic material (0-3%). Because soil character strongly influences hydrologic properties (Lohse and Dietrich, 2005), the similarity in soil texture at all study sites suggests that study hillslopes likely exhibit similar hydrologic properties. Due to the limited variability in soil texture across the study region, these results cannot be used to draw conclusions regarding the importance of soil texture on debris flow initiation and soil texture cannot be used to predict debris flow hazard in RMNP.

5.2.3 Topography

Significant differences in the proportion of field-based categorizations of slope morphology (slope convergence and the presence of colluvial hollows) indicate that local slope morphology influences the likelihood of debris flow occurrence. Hillslopes with a colluvial hollow or other forms of convergent topography occurred more frequently at debris flow sites than control sites by over 30%. This difference likely reflects the fact that convergent sites are better able to

accumulate surface water and groundwater flow (Condon and Maxwell, 2015) and concentrate unconsolidated source material, a necessary factor for debris flow initiation (Lumb, 1975; Costa, 1984). Because slope failure requires that gravitational forces overcome the internal cohesion of the material (Iverson, 1997, 2014), increasing saturation and pore fluid pressure by accumulated soil moisture logically increases the susceptibility of a hillslope to debris flow failure.

The relatively coarse DEM resolution (10 m) and small drainage size of the study sites limited accuracy of remote topographic characterizations. The limited descriptive power of remotely calculated curvature values is demonstrated by the fact that planform curvature scores do not align with field classifications of slope morphology. Slope curvature calculated using a 10 m DEM was not significantly different between site types and could not be used to accurately predict site type, indicating that remote classifications of slope curvature with a 10 m DEM cannot be used to assess debris flow hazard in RMNP. Because curvature scores are relative and dimensionless, it is difficult to assess how well the calculated score reflects site conditions. It is possible, however, that higher resolution topographic imagery would improve accuracy of these scores and the predictive value of remotely calculated curvature.

Remotely calculated contributing area was not significantly different at debris flow sites and control sites and demonstrated minimal efficacy in predicting debris flow occurrence. As described above, the resolution of topographic imagery may limit the accuracy of remote calculations in small drainage areas. Unlike the curvature scores, however, topographic maps and satellite imagery were used to manually verify the watershed polygons generated for these calculations. At all study sites, calculated drainage area appeared to describe local topography

successfully. As such, contributing area cannot be clearly linked to debris flow occurrence and cannot be used to assess debris flow hazard in RMNP, despite its inclusion in the logistic lasso regression model.

5.2.4 Vegetation

Dependency of debris flow occurrence and vegetation type was not observed for the study sites in RMNP, indicating that vegetation cover cannot be used to asses debris flow hazard in this region. These results may indicate that vegetation type is not an important controlling variable on debris flow initiation, that a three-factor categorization did not adequately describe site conditions, or that the sample size was not large enough to distinguish differences in vegetation.

5.2.5 Fire history

As only one of the debris flow sites occurred in an area that has experienced a documented wildfire within the last 60 years, and because this site did not deviate from other observed patterns of controlling variables on debris flow occurrence (i.e., slope convergence), Hypothesis 2 cannot be substantiated with the debris flow sites studied here. Despite an extensive body of literature demonstrating that fire occurrence increases susceptibility to slope failure by altering groundwater and surface water hydrology (Swanson, 1981; Cannon et al., 2001; Wondzell and King, 2003; Goode et al., 2012; Nyman et al., 2013), debris flow occurrence in RMNP following the 2013 storm does not appear to be strongly linked to fire history. These findings are consistent with surveys of other 2013 debris flows that occurred elsewhere in Colorado (Anderson et al., 2015), and indicate that slope failures during this event are best attributed to soil saturation rather than fire-induced changes to soil hydrology.

5.2.6 Logistic regression

Although both logistic regression techniques accurately predicted greater than 50% of the test data, neither demonstrate significant potential for applications in debris flow prediction. In particular, the logistic lasso regression did not predict debris flows, correctly or incorrectly, in any of the six test cases, and would only predict slope failure in the case of extremely large contributing areas. Predictions of debris flow by this model are most likely driven not by realistic correlation with debris flow occurrence in large drainage areas, but rather a single debris flow in the training dataset (North St. Vrain) that has an unusually large contributing area. This model is therefore of little use to land managers.

The LDA model, which demonstrated a similar total test error rate (4 of 6 sites), did correctly predict one of the two debris flows, and therefore may be of slightly greater use in predictions of debris flow locations in the case of a large rain storm. However, due to number of debris flows and the subsequently small test dataset, it is difficult to accurately gauge the effectiveness of this model or the relative importance of the covariates included in LDA analysis. Models of this nature, although they may be useful tools to indicate potential areas of greater hazard, would not be appropriate tools to indicate debris flow hazard without substantial field assessment and detailed characterization of slope conditions.

5.3 Debris flow chronology

Although numeric ages of older debris flow deposits at the Bighorn debris flow site are not conclusive, field mapping, stratigraphic exposure, and diffusion of old deposits confirm that at least two and likely three older debris flows occurred at this site before the 2013 event. Objective

1 to complete a detailed geochronology of debris flows is therefore limited to a relative chronology of the 2-3 well preserved old deposits identified at the Bighorn debris flow site. The presence of multiple debris flow deposits at this site indicates that replenishment of unconsolidated material in the colluvial hollow above the failure site would allow for future debris flows in the Bighorn Creek drainage.

5.3.1 Deposit mapping

Mapping of the older debris flow levees at the Bighorn debris flow site confirms that two or three levee-depositing debris flows have occurred in the Bighorn Creek drainage. It is possible that additional flows that did not deposit levees have also occurred at this site, as is indicated by the relatively young (468 years BP) radiocarbon sample collected from the trench exposure. Based on qualitative observations, the oldest debris deposits, those farthest outset from the 2013 debris channel, exhibit the greatest degree of surficial weathering. The recurrence of debris flow events at this site indicates that the colluvial hollow above the 2013 scarp accumulates unconsolidated material and periodically flushes this material in debris flows when thresholds of sediment volume and substrate saturation are met.

5.3.2 Stratigraphy

Stratigraphic exposure in the excavated trench corroborates field mapping of at least two older debris flows at the Bighorn debris flow site. At least two packages of debris flow material were identified in this trench, as well as a hyper-concentrated flow deposit directly overlying the younger of these debris flow deposits. The hyper-concentrated flow may have occurred immediately following deposition of the underlying debris deposit as runoff reworked sediment

and re-entrained fine grained material. Coupling of these strata is likely, as debris is commonly reworked by the fluidized, watery tails of debris flows, which are typically able to winnow finer sediment from the upslope portions of a deposit (Costa, 1984; Iverson, 2014). Alternatively, all three deposits exposed in this trench may represent temporally distinct events.

Because the base of the trench did not reach bedrock, and because of the spatially discontinuous nature of debris fans, it is likely that additional old debris flow deposits exist at the Bighorn debris flow site but were not exposed in the excavated trench.

5.3.3 Radiocarbon analysis

Because none of the radiocarbon ages determined for old debris deposits correspond to each other or other numeric ages, it is difficult to determine the exact age of old debris deposits at the Bighorn debris flow site. In fact, some of the radiocarbon ages conflict with relative ages determined through deposit mapping, indicating that at least some of the measured radiocarbon ages are not representative of deposit age.

All of the measured ^{14}C ages are on the order of one to several hundred years before 2013 (983 radiocarbon years to modern) and indicate that debris deposits at this site are at least several hundred years old. It is unlikely that debris flows have occurred more recently than these ages suggest, which would require preservation of small fragments of older organic material. It is, however, likely that debris deposits containing carbon samples occurred prior to the years determined through radiocarbon analysis, as the samples characterized as "fair" include samples of organic material that may have been younger root material. Additionally, the "good" or

"excellent" samples that were found pinned between large boulders may have been trapped in place by isolated boulder movements after the main debris flow deposit was emplaced. Thus, although they do not provide conclusive absolute ages of old debris flow deposits, radiocarbon ages do indicate the dynamic nature of the steep hillslope environment at the Bighorn debris flow site and demonstrate the difficulty of dating landforms in debris flow environments.

5.3.4 Lichenometry

Although difference in lichen colony diameters is not sufficient to establish relative ages of levees 1 and 2 without an established growth curve or a better knowledge of the species measured in the field, the older age of levee 2 indicated by larger lichen colonies corroborates the relative age of these levees determined by other geochronologic techniques, including the spatial relationship of these levees and ^{10}Be exposure age of Levee 3 relative to Levees 1 and 2.

5.3.5 Dendrochronology

Tree ring analysis indicates that scarring of the sampled tree occurred 172 years before 2013. This date does not align with numeric ages established for levee 1 using other geochronologic techniques and indicates a younger event than is suggested by other techniques. Because only one tree wedge was available for analysis, this date cannot be conclusively linked to a debris flow; without other data to corroborate the age of the event that scarred the tree, it is unclear if the scar resulted from a mass movement, an isolated boulder moving downslope, or another cause.

5.3.6 Cosmogenic exposure ages

Substantial inheritance is implied by the ^{10}Be cosmogenic radionuclide data. The 2013 boulder sample, which should have returned a zero exposure age, instead returned an 18.1 ka exposure age, indicating an equivalent of 18.1 thousand years of ^{10}Be inheritance for that sample. By subtracting the minimum exposure age from the maximum age calculated for each levee, total inheritance is at least 54.2, 143, and 121 thousand years for levees 1, 2, and 3, respectively. These large inheritance values indicate that the surfaces of boulders transported short distances (0.5-1.0 km) in a debris flow are not sufficiently scoured to "re-set" the exposure age of large clasts. This finding is corroborated by field observations that some boulders deposited in the 2013 debris flow still had patchy lichen coverage on protected faces, particularly in the upper portion of the debris channel near the failure scarp. Furthermore, samples collected from levee 2 returned apparently younger exposure ages, which may reflect that those samples were collected farther downslope and therefore experienced greater transport.

These inherited ages and field observations may indicate that exposure dating may not be as applicable to debris flows as to rockfall events. Although rockfall exposes entirely fresh faces and commonly orients the fresh faces upright (Mackey and Quigley, 2014), the ^{10}Be dates obtained in this study indicate that debris flow material does not demonstrate a reliable statistical arrangement of surfaces with no previous atmospheric exposure. As such, debris flow deposits may not be appropriate candidates for exposure dating.

The samples collected from the outermost Levee 3 do show the generally oldest exposure ages. These results correspond to the interpretation that deposition of the outermost levee (Levee 3)

must pre-date deposition of the levees closer to the center of the valley (Levees 1 and 2) based on field relationships and surficial weathering. The ^{10}Be exposure data therefore corroborate the relative chronology determined using the dating techniques described in the preceding sections. Larger sample sizes of boulders from each of the older levees might allow for confirmation that clasts in Levee 3 have been exposed to the atmosphere longer and therefore might allow for significant tests indicating relative ages of the old levee deposits at this site. Using the difference in means between Levee 1 and Levee 3 (66.6 ka) and the average standard deviation of both groups (44.8 ka), an 80% power calculation with 95% confidence indicates that a sample size of n = 8 would have been necessary to determine a significant difference in the age of these deposits for use in relative dating.

It is theoretically possible that a large number of ^{10}Be samples collected from the 2013 debris flow levee at the Bighorn site might allow for estimation of a correction factor using the mean inherited age of boulders transported in the 2013 debris flow. Correction of inherited radionuclide exposure ages has been suggested for debris flow deposits in Prospect Canyon on the Colorado River (Cerling et al., 1999). Successful use of an inheritance correction factor, however, would require a large enough sample of boulders from both the old and modern deposits to create a statistically significant correction. To demonstrate the sample sizes that would be needed to create a statistically significant correction factor, Figure 5.1 shows a series of power calculations generated for two-sample tests between a modern debris flow levee and an older deposit. In this case, the difference in means used in the power calculation (σ) would equal the true age of the old deposit. The standard deviation was estimated using the standard deviation of exposure ages measured from Levee 1 (24.1 ka). Due to the localized nature of inheritance

histories, however, any correction factor of this kind would be limited in its application beyond the Bighorn debris flow site.

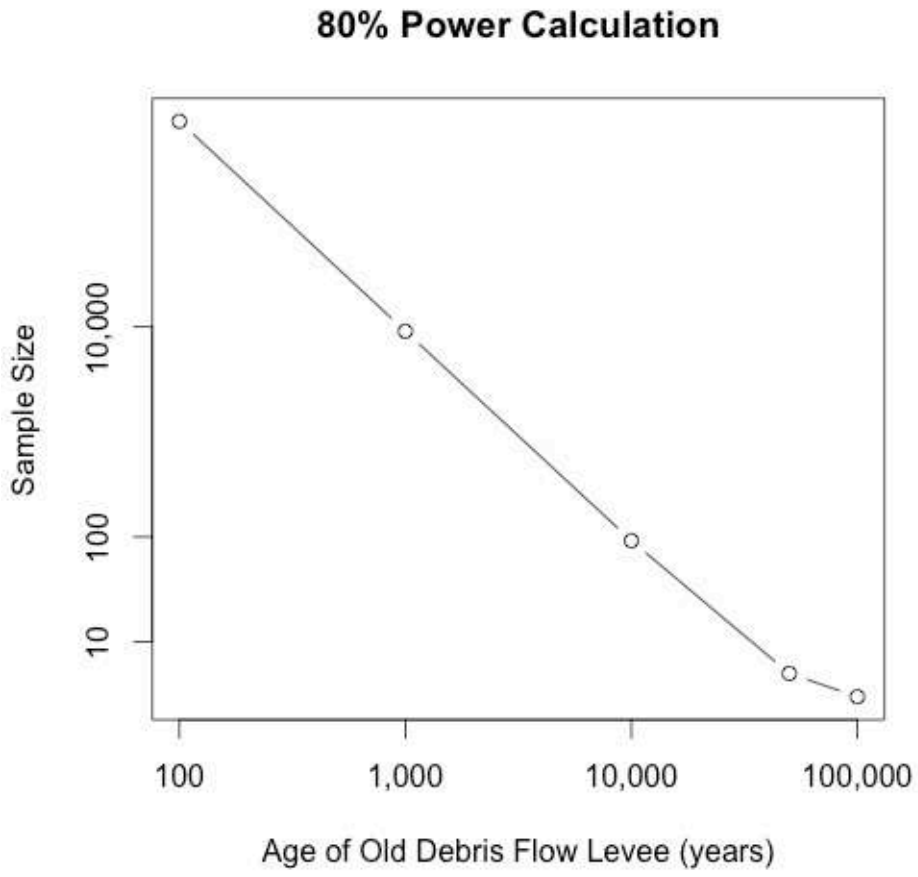

Figure 5.1. Plot showing necessary sample size power to run a two sample t-test for cosmogenic exposure ages collected from a modern levee and an older levee with 95% confidence and 80% power. Standard deviation was estimated from the standard deviation in exposure ages collected from Levee 1 (σ = 24.1 ka). Axes are shown on a logarithmic scale.

As is indicated by Figure 5.1, the necessary samples sizes indicated by these power calculations are greater than 100 for deposits < 10,000 years old. Aside from budgetary constraints, sampling at this scale is not likely feasible because debris deposits, at the Bighorn site and elsewhere in RMNP, are spatially limited and may not include sufficient numbers of appropriate boulders to

sample. Use of a correction factor in this manner would therefore only be possible in cases where prior study indicates that a debris flow deposit is > 10,000 years old, preferably older.

5.3.6 Debris flow chronology and climatic forcing

An extensive body of research links debris flow activity to paraglacial response following retreat of glacial ice (e.g., Eisbacher and Clague, 1994; Evans and Clague, 1994; Solomina et al., 1994; Menounos, 2000; Ballantyne, 2002a, 2002b; Reid and Thomas, 2006). It is therefore possible that debris flow deposits at the Bighorn debris flow site occurred after the Pinedale (30-12 ka) or Bull Lake (150-130 ka) glaciations. The numeric ages of old debris deposits determined in this study, which are limited in both precision and accuracy, do not correspond exactly with the conclusion of either glacial period. However, the cosmogenic exposure ages do suggest deposit ages on the same order of magnitude as the end of both glaciations. Most notably, Levees 1 and 2 are characterized by minimum exposure ages of 30 ka and 8 ka, respectively, and may be linked to climatic changes during and after the Pinedale Glaciation. Debris flow activity during this time would align with an increased debris flow likelihood suggested by Menounos (2000) between 9-6 ka that resulted from the onset of summer monsoonal weather during the Holocene. It is therefore possible that debris flows at this site occurred in connection with climate amelioration and paraglacial landscape adjustment after one or both glaciations. Alternatively, radiocarbon ages indicate sediment movement on the order of 100-1000 years, which may correspond to climatic shifts during the main stage of the Little Ice Age (1600-1870 AD).

6. CONCLUSIONS

During the fall 2013 rainstorm in the Colorado Front Range, more than 10 debris flows that occurred in RMNP delivered large sediment loads to valley bottoms and had the potential to injure park staff and visitors and damage infrastructure. Numerous smaller slope failures also occurred throughout the area. These mass movements underscore the potential for debris flow hazards in RMNP and surrounding communities. Future management of infrastructure and human activity in this region must acknowledge potential risks from debris flows.

6.1 Controls on debris flow initiation

Regional variables, including elevation, climate, and slope angle, are well-established controls on debris flow initiation, but do not fully explain the spatial distribution of debris flows within a landscape subject to all of these controls. This study demonstrates a clear link between debris flow occurrence and site-specific slope morphology, including slope convergence and the presence of colluvial hollows. Debris flow occurrence, however, is controlled by a complex interaction of geomorphic and climate variables across all spatial and temporal scales. Conclusions regarding the influence of most site-specific variables measured in this study are limited. Many of the geomorphic variables measured for comparison in this study, including soil depth, remote topographic characterization, and vegetation cover, are likely important controls on debris flow initiation that were not adequately described in this study. Other possible data limitations include difficulty accurately measuring slope conditions and the interaction of variables that were not analyzed in this study.

As described in the discussion sections above, slope convergence and the presence of colluvial hollows correspond to debris flow occurrence in RMNP when assessed on a localized scale. Low-resolution metrics of slope morphology, however, did not align with field observations to capture the subtleties of convergence in small RMNP drainages. As such, local debris flow hazard assessments must include field characterization of hillslopes. It is possible that higher resolution topographic data could provide better indication of debris flow susceptibility, although the value of high-resolution data in remote slope characterization and hazard assessment remains to be evaluated in this region. Until such an evaluation is conducted, observations of slope convergence and debris flow deposits at a site are good indicators that a slope may experience debris flows in the future. Management of buildings, infrastructure, and human activity in such areas must acknowledge a level of debris flow risk that cannot be quantified with existing data.

6.2 Spatial and temporal distribution of debris flows in RMNP

In addition to identifying site-specific geomorphic controls on debris flow initiation, this study also attempted to describe the temporal distribution of debris flows in RMNP in order to determine whether the 2013 rainstorm and resulting debris flows were anomalous on either human or geologic timescales. Relative geochronologic techniques demonstrate that some hillslopes in RMNP, such as the Bighorn debris flow site, have experienced recurrent debris flows within the last 10^2-10^3 years. Although infrequent on a human timescale, debris flows triggered by extreme rainfall, at least in localized areas, are therefore not unprecedented in the geologic record. It is unclear whether the extensive spatial scale of the 2013 debris flow event is anomalous in this region, but the possibility that such an event will occur again on a human timescale cannot be discounted.

6.3 Understanding dynamic debris flow landscapes

Application of geochronologic techniques in this study clearly demonstrates the dynamic nature of steep hillslopes and debris flow landscapes. The specific histories of organic and inorganic material within debris flow deposits, including initial exhumation of parent material, residence in sinks along the hillslope, and final deposition by a debris flow, are not easily described by standard dating techniques. Particle histories are highly specific to a given hillslope and even to the individual particles within a flow. Measures of sediment exposure age, including lichenometry and radionuclide dating, are therefore limited in their ability to date old debris deposits and account for inherited exposure, particularly when sample sizes are small.

Post-debris flow histories further complicate the re-creation of sediment pathways; gradual diffusion and alteration of debris deposits by water, gravitational, and biologic processes can dramatically alter the deposit and introduce organic material not originally deposited by the debris flow, as is evinced by modern and apparently young ^{14}C ages measured in this study.

The difficulty in accurately dating debris deposits is testament to the complex and dramatic natural history of high-relief landscapes. A better understanding of the subtleties of the spatial and temporal debris flow distribution on steep hillslopes necessitates a holistic perspective of the many geomorphic processes that interact to produce the necessary conditions for slope failure.

6.4 Implications for management

Because this study was not able to identify remote slope measurements that correlate with debris flow occurrence, Objective 2 to conduct a landscape analysis in RMNP cannot be meaningfully completed. However, this study does allow for a few general management recommendations:

1. Areas of convergent topography, and particularly hillslopes immediately below a colluvial hollow, are most susceptible to debris flow failure. As such, buildings, infrastructure, and people on these hillslopes and in the valleys below are at greater risk for damage by debris flows than on hillslopes not characterized by convergence. When possible, plans for future buildings and infrastructure should therefore avoid areas on or below hillslopes with convergent topography. The colluvial hollows that sourced 2013 debris flows are not clearly identifiable in Google Earth Imagery. However, steep rocky outcroppings that are visible in aerial imagery (including Lumpy Ridge, McGregor Mountain, and other cliff-forming locations) may form hollows more readily and could be prioritized for hazards assessment.

2. The recurrence of debris flows at the Bighorn debris flow site indicates that the colluvial hollow above the 2013 scarp may source debris flows in the future and deliver additional debris flow sediment to the fan below in a potentially destructive manner. As such, the Bighorn Ranger Station and the surrounding infrastructure are at some risk of damage by future debris flows. A precise recurrence interval of debris flows at the Bighorn debris flow sites could not be determined. However, the anomalously large magnitude of the 2013 rainstorm that triggered failure and the interpretation of periodic filling and flushing

of the colluvial hollow at this site suggest that, although possible, destructive debris flows at this site are not probable in the immediate future.

3. As was demonstrated most clearly by the Bighorn debris flow, slopes in RMNP that have experienced past debris flows can generate more than one slope failure through time. As such, areas of known debris flow occurrence, such as pre-existing debris fans and debris flow channels, may source future debris flows when other conditions for debris flow initiation (soil saturation) are met. When possible, plans for future buildings and infrastructure should avoid areas on or below hillslopes with known debris flow deposits.

4. Results of this research demonstrate that topographic variables are important controls on debris flow initiation. The topographic metrics calculated from 10 m DEMs, however, were not linked to debris flow occurrence. These conclusions indicate that low resolution topographic data limits the ability to assess debris flow hazards. Production of high-resolution topographic imagery, such as 1 m DEMs or LiDAR data may improve the ability to remotely estimate debris flow risk.

6.5 Ideas for future research

This research highlights a number of topics for further study that would improve understanding of spatial and temporal patterns in debris flow initiation in the Colorado Front Range.

6.5.1 Geomorphic controls

As discussed above, soil depth measurements were poorly representative of true thickness of unconsolidated material. Rather than rely upon mechanical measurements, characterization of soil depth would be improved through use of geophysical techniques including GPR or electrical resistivity. Better measurement of soil depth, as well as the cross-sectional resolution that geophysical lines would provide, would allow for better comparison of soil depth patterns at failed and unfailed hillslopes within RMNP.

6.5.2 Geochronology

The relative chronology of debris flow deposits at the Bighorn debris flow site established in this study has highlighted the need for better understanding of the frequency of debris flows at this site. Although the numeric dating techniques employed in this research did not yield conclusive ages, it is possible that more targeted collection of tree-ring and carbon samples could be used to better constrain the ages of old deposits. Previous study has successfully dated deposits in debris fans using organic material (Cerling et al., 1999). It is also possible that radiocarbon dating of organic material collected from the debris fan, rather than debris levees, would be less subject to secondary slope processes and could be used to date older debris deposits. The availability of organic material, however, may limit further application of radiocarbon dating at the Bighorn site. In areas with greater frequency of mass movements, dendrochronology has also been used to determine the age of debris fans (Wilford et al., 2005; Koch et al., 2014; Schraml et al., 2015). A more expansive dencrochronologic survey of trees on the debris fan at the Bighorn debris flow site may yield successful control on the ages of debris flows at this site. Alternatively, optically

stimulated luminescence dating (OSL) could yield more robust ages of sandy debris deposits by dating time since burial (up to 350 ka) of quartz and feldspar sand (Murray and Olley, 2002).

Additionally, other relative techniques including the degree of soil formation (Menounos, 2000) and models of levee diffusion could be calibrated in the region. Calibrations of these relative techniques would require comparison with debris flow surfaces of known age elsewhere in the Colorado Front Range, including a geochronologic assessment of debris deposits near Sky Pond, Colorado (Menounos, 2000) and other debris deposits of known age.

REFERENCES

Anderson, S.W., Anderson, S.P., and Anderson, R.S., 2015, Exhumation by debris flows in the 2013 Colorado Front Range storm: Geology, v. 43, p. 1–4, doi: 10.1130/G36507.1.

Baker, W.L., 2009, Fire Ecology in Rocky Mountain Landscapes: Island Press, 625 p.

Balco, G. CRONUS-Earth online calculators: 2008.

Ballantyne, C.K., 2002a, A general model of paraglacial landscape response: The Holocene, p. 371–376.

Ballantyne, C.K., 2002b, Paraglacial Geomorphology: Quaternary Science Reviews, v. 21, p. 1935–2007.

Benedict, J.B., 1967, Recent glacial history of an alpine area in the Colorado Front Range, USA, Establishing a lichen-growth curve: Journal of Glaciology, v. 6, p. 817–832.

Birkeland, P.W., 1999, Soils and Geomorphology: New York, Oxford University Press.

Birkeland, P.W., Shroba, R.R., Burns, S.F., Price, a. B., and Tonkin, P.J., 2003, Integrating soils and geomorphology in mountains - An example from the Front Range of Colorado: Geomorphology, v. 55, p. 329–344, doi: 10.1016/S0169-555X(03)00148-X.

Braddock, W., and Cole, J., 1990, Geologic Map of Rocky Mountain National Park and Vicinity:.

Buechling, A., and Baker, W.L., 2004, A fire history from tree rings in a high-elevation forest of Rocky Mountain National Park: Canadian Journal of Forest Research, v. 34, p. 1259–1273, doi: 10.1139/x04-012.

Bull, W.B., 1996, Dating San Andreas fault earthquakes with lichenometry Dating San Andreas fault earthquakes with lichenometry: , p. 111–114, doi: 10.1130/0091-7613(1996)024<0111.

Caine, N., 1984, Elevational contrasts in contemporary geomorphic activity in the Colorado Front Range: Studia Geomorphologica Carpatho-Balcania, v. 18, p. 5–31.

Cannon, S.H., Kirkham, R.M., and Parise, M., 2001, Wildfire-related debris-flow initiation processes, Storm King Mountain, Colorado: Geomorphology, v. 39, p. 171–188, doi: 10.1016/S0169-555X(00)00108-2.

Cerling, T.E., Webb, R.H., Poreda, R.J., Rigby, A.D., and Melis, T.S., 1999, Cosmogenic 3He ages and frequency of late Holocene debris flows from Prospect Canyon, Grand Canyon, USA: Geomorphology, v. 27, p. 93–111, doi: 10.1016/S0169-555X(98)00092-0.

Coe, J.A., 2015, Personal Communication:.

Coe, J.A., Kean, J.W., Godt, J.W., Baum, R.L., Jones, E.S., Gochis, D.J., and Anderson, G.S., 2014, New insights into debris-flow hazards from an extraordinary event in the Colorado Front Range: GSA Today, v. 24, p. 4–10, doi: 10.1130/GSATG214A.1.

Coe, J. a., Kinner, D. a., and Godt, J.W., 2008, Initiation conditions for debris flows generated by runoff at Chalk Cliffs, central Colorado: Geomorphology, v. 96, p. 270–297, doi: 10.1016/j.geomorph.2007.03.017.

Colorado Climate Center Climate of Colorado:.

Condon, L.E., and Maxwell, R.M., 2015, Evaluating the relationship between topography and groundwater using outputs from a continental-scale integrated hydrology model: Water Resources Research, v. 51, p. 6602–6621, doi: 10.1002/2014WR016774.

Costa, J.E., 1984, Physical geomorphology of debris flows, *in* Costa, J.E. and Fleisher, J.P. eds., Developments and Applications of Geomorphology, Springer-Verlag, p. 268–312.

Costa, J.E., and Jarrett, R.D., 1981, Debris flows in small mountain stream channels of Colorado and their hydrologic implications: Bulletin of the Association of Engineering Geologists, v. 18, p. 309–322.

Eisbacher, G.H., and Clague, J.J., 1994, Destructive Mass Movements in High Mountains: Hazard and Management:.

Evans, S.G., and Clague, J.J., 1994, Recent climatic change and catastrophic geomorphic processes in mountain environments: Geomorphology, v. 10, p. 107–128, doi: 10.1016/0169-555X(94)90011-6.

Final Master Plan, 1976,.

Frank, F., McArdell, B.W., Huggel, C., and Vieli, A., 2015, The importance of entrainment and bulking on debris flow runout modeling: examples from the Swiss Alps: Natural Hazards and Earth System Sciences, v. 15, p. 2569–2583, doi: 10.5194/nhess-15-2569-2015.

Gochis, D., Schumacher, R., Friedrich, K., Doesken, N., Kelsch, M., Sun, J., Ikeda, K., Lindsey, D., Wood, A., Dolan, B., Matrosov, S., Newman, A., Mahoney, K., Rutledge, S., et al., 2015, The great Colorado flood of September 2013: Bulletin of the American Meteorological Society, v. 96, p. 1461–1487, doi: 10.1175/BAMS-D-13-00241.1.

Godt, J.W., and Coe, J. a., 2007, Alpine debris flows triggered by a 28 July 1999 thunderstorm in the central Front Range, Colorado: Geomorphology, v. 84, p. 80–97, doi: 10.1016/j.geomorph.2006.07.009.

Godt, J.W., Coe, J. a, Kean, J.W., Baum, R.L., Jones, E.S., Harp, E.L., Staley, D.M., and Barnhart, W.D., 2014, Landslides in the Northern Colorado Front Range Caused\rby Rainfall, September 11–13, 2013: USGS Fact Sheet 2013–3114,.

Goode, J.R., Luce, C.H., and Buffington, J.M., 2012, Enhanced sediment delivery in a changing climate in semi-arid mountain basins: Implications for water resource management and aquatic habitat in the northern Rocky Mountains: Geomorphology, v. 139-140, p. 1–15, doi: 10.1016/j.geomorph.2011.06.021.

Granger, D.E., Lifton, N.A., and Willenbring, J.K., 2013, A cosmic trip: 25 years of cosmogenic nuclides in geology: Geological Society of America Bulletin, v. 125, p. 1379–1402, doi: 10.1130/B30774.1.

Grimsley, K.J., Rathburn, S.L., Friedman, J.M., and Mangano, J.F., 2016, Debris Flow Occurrence and Sediment Persistence, Upper Colorado River Valley, CO: Environmental Management, doi: 10.1007/s00267-016-0695-1.

Guthrie, R.H., Hockin, a., Colquhoun, L., Nagy, T., Evans, S.G., and Ayles, C., 2010, An examination of controls on debris flow mobility: Evidence from coastal British Columbia: Geomorphology, v. 114, p. 601–613, doi: 10.1016/j.geomorph.2009.09.021.

de Haas, T., Braat, L., Leuven, J.R.F.W., Lokhorst, I.R., and Kleinhans, M.G., 2015, Effects of debris flow composition on runout, depositional mechanisms, and deposit morphology in laboratory experiments: Journal of Geophysical Research: Earth Surface, v. 120, p. 1949–1972, doi: 10.1002/2015JF003525.

Huggel, C., 2009, Recent extreme slope failures in glacial environments: effects of thermal perturbation: Quaternary Science Reviews, v. 28, p. 1119–1130, doi: 10.1016/j.quascirev.2008.06.007.

Iverson, R.M., 2014, Debris flows: behaviour and hazard assessment: Geology Today, v. 30, p. 15–20.

Iverson, R.M., 1997, The physics of debris flows: Reviews of Geophysics, v. 35, p. 245–296.

Iverson, R.M., Reid, M.E., Logan, M., LaHusen, R.G., Godt, J.W., and Griswold, J.P., 2010, Positive feedback and momentum growth during debris-flow entrainment of wet bed sediment: Nature Geoscience, v. 4, p. 116–121, doi: 10.1038/ngeo1040.

KellerLynn, K., 2004, Rocky Mountain National Park Geologic Resource Evaluation Report:.

Kimerling, J.A., Buckley, A.R., Muehrcke, P.C., and Muehrcke, J.O., 2011, Map Use: Reading Analysis Interpretation: ESRI Press Academic, 610 p.

Klos, P.Z., Link, T.E., and Abatzoglou, J.T., 2014, Extent of the rain-snow transition zone in the western U.S. under historic and projected climate: Geophysical Research Letters, p. n/a–n/a, doi: 10.1002/2014GL060500.

Koch, J., Clague, J.J., and Blais-Stevens, A., 2014, Debris flow chronology and potential hazard along the Alaska highway in Southwest Yukon territory: Environmental and Engineering Geoscience, v. 20, p. 25–43, doi: 10.2113/gseegeosci.20.1.25.

Lohse, K.A., and Dietrich, W.E., 2005, Contrasting effects of soil development on hydrological properties and flow paths: Water Resources Research, v. 41, p. n/a–n/a, doi: 10.1029/2004WR003403.

LTI TruPulse 360 / 360B User's Manual 2nd Edition, 2009,.

Lumb, P., 1975, Slope failures in Hong Kong: Quarterly Journal of Engineering Geology, v. 8, p. 31–65.

Mackey, B.H., and Quigley, M.C., 2014, Strong proximal earthquakes revealed by cosmogenic 3He dating of prehistoric rockfalls, Christchurch, New Zealand: Geology, v. 42, p. 975–978, doi: 10.1130/G36149.1.

Madole, R.F., VanSistine, D.P., and Michael, J.A., 1998, Pleistocene glaciation in the upper Platte River drainage basin, Colorado:.

Megahan, W.F., 1983, Hydrologic effects of clearcutting and wildfire on steep granitic slopes in Idaho: Water Resources Research, v. 19, p. 811–819, doi: 10.1029/WR019i003p00811.

Menounos, B., 2000, A Holocene debris-flow chronology for an alpine catchment, Colorado Front Range, *in* Slaymaker, O. ed., Geomorphology, Human Activity, and Global Environmental Change, John Wiley & Sons, p. 117–149.

Murray, A.S., and Olley, J.M., 2002, Precision and accuracy in the optically stimulated luminescence dating of sedimentary quartz: A status review: Geochronometria, v. 21, p. 1–16.

Nishiizumi, K., Imamura, M., Caffee, M.W., Southon, J.R., Finkel, R.C., and McAninch, J., 2007, Absolute calibration of 10Be AMS standards: Nuclear Instruments and Methods in Physics Research Section B: Beam Interactions with Materials and Atoms, v. 258, p. 403–413, doi: 10.1016/j.nimb.2007.01.297.

Nyman, P., Sheridan, G.J., and Lane, P.N.J., 2013, Hydro-geomorphic response models for burned areas and their applications in land management: Progress in Physical Geography, v. 37, p. 787–812, doi: 10.1177/0309133313508802.

Ott, R.L., and Longnecker, M., 2010, An Introduction to Statistical Methods and Data Analysis: Belmont, CA, Brooks/Cole, Cengage Learning.

Pierson, T.C., 2005, Distinguishing between Debris Flows and Floods from Field Evidence in Small Watersheds: USGS Fact Sheet 2004-3142,.

Rathburn, S.L., Rubin, Z.K., and Wohl, E.E., 2013, Evaluating channel response to an extreme sedimentation event in the context of historical range of variability: Upper Colorado River, USA: Earth Surface Processes and Landforms, v. 38, p. 391–406, doi: 10.1002/esp.3329.

Reid, E., and Thomas, M.F., 2006, A chronostratigraphy of mid- and late-Holocene slope evolution: Creagan a' Chaorainn, Northern Highlands, Scotland: Holocene, v. 16, p. 429–444, doi: 10.1191/0959683606hl939rp.

Schraml, K., Oismueller, M., Stoffel, M., Huebl, J., and Kaitna, R., 2015, Debris-flow activity in five adjacent gullies in a limestone mountain range: Geochronometria, v. 42, p. 60–66, doi: 10.1515/geochr-2015-0007.

Schuster, R.L., and Highland, L.M., 2007, Overview of the Effects of Mass Wasting on the Natural Environment: Environmental and Engineering Geoscience, v. 13, p. 25–44, doi: 10.2113/gseegeosci.13.1.25.

Schutte, M., Pitlick, J., and Neupauer, R., 2014, Geomorphic response of Roaring River and Fall River to the September 2013 flood, *in* AGU Abstracts with Programs, San Fransisco, CA.

Sibold, J.S., Veblen, T.T., and Gonzalez, M.E., 2006, Spatial and temporal variation in historic fire regimes in subalpine forests across the Colorado Front Range in Rocky Mountain National Park, Colorado, USA: Journal of Biogeography, v. 33, p. 631–647, doi: 10.1111/j.1365-2699.2005.01404.x.

Sibold, J.S., Veblen, T.T., and González, M.E., 2006, Spatial and temporal variation in historic fire regimes in subalpine forests across the Colorado Front Range in Rocky Mountain National Park, Colorado, USA: Journal of Biogeography, v. 33, p. 631–647, doi: 10.1111/j.1365-2699.2005.01404.x.

Solomina, O.N., Savoskul, O.S., and Cherkinsky, a. E., 1994, Glacier variations, mudflow activity and landscape development in the Aksay Valley (Tian Shan) during the late Holocene: The Holocene, v. 4, p. 25–31, doi: 10.1177/095968369400400104.

Stock, J.D., and Dietrich, W.E., 2006, Erosion of steepland valleys by debris flows: Bulletin of the Geological Society of America, v. 118, p. 1125–1148, doi: 10.1130/B25902.1.

Stoffel, M., Butler, D.R., and Corona, C., 2013, Mass movements and tree rings: A guide to dendrogeomorphic field sampling and dating: Geomorphology, v. 200, p. 106–120, doi: 10.1016/j.geomorph.2012.12.017.

Swanson, F.J., 1981, Fire and geomorphic processes, *in* Mooney, H.A., Bonnickson, T.M., Christensen, N.L., Lotan, J.E., and Reiners, W.A. eds., Fire regimes and ecosystem properties, USDA Forest Service General Technical Report, p. 401–420.

Whipple, K.X., and Dunne, T., 1992, The influence of debris-flow rheology on fan morphology, Owens Valley, California: Geological Society of America Bulletin, v. 104, p. 887–900, doi: 10.1130/0016-7606(1992)104<0887:TIODFR>2.3.CO;2.

Wilford, D., Cherubini, P., and Sakals, M., 2005, Dendroecology A Guide for Using Trees to Date Geomorphic and Hydrologic Events Dendroecology A Guide for Using Trees to Date Geomorphic and Hydrologic Events: British Columbia Ministry of Forests, Forest Science Program Handbook No. 58., doi: 10.1016/j.landurbplan.2008.05.003.

Wondzell, S.M., and King, J.G., 2003, Postfire erosional processes in the Pacific Northwest and Rocky Mountain regions: Forest Ecology and Management, v. 178, p. 75–87, doi: 10.1016/S0378-1127(03)00054-9.

APPENDIX A

Table A.1. Site data for all 41 sites included in this study.

Name	Elevation (m)	Aspect (deg)	Slope (m/m)	Longitude	Latitude
NDF1	2,573	172.88	60.47	-105.59465	40.34625
NDF2	2,684	213.44	79.39	-105.54292	40.41084
NDF4	3,199	187.59	75.66	-105.57300	40.27523
NDF5	3,191	324.46	43.01	-105.65213	40.38494
NDF6	2,870	15.26	57.01	-105.63126	40.38905
NDF7	2,827	221.57	88.55	-105.58710	40.37590
NDF8	2,606	173.66	45.28	-105.53886	40.22120
NDF9	2,590	180.00	40.00	-105.56892	40.37627
NDF10	2,685	180.00	92.50	-105.51525	40.43403
NDF11	2,552	45.00	54.80	-105.54871	40.40227
NDF12	2,819	155.56	75.52	-105.63762	40.41478
NDF13	2,614	248.50	46.67	-105.57896	40.35693
NDF14	2,733	128.09	58.76	-105.56260	40.21341
NDF16	3,187	151.70	55.37	-105.56634	40.29300
NDF17	2,806	167.47	46.10	-105.61658	40.32469
NDF18	2,812	162.30	64.06	-105.62528	40.32308
NDF19	2,751	12.99	50.03	-105.59108	40.39182
NDF20	2,695	223.36	61.90	-105.57283	40.40479
NDF21	2,936	212.20	79.77	-105.65310	40.41806
NDF23	2,622	124.51	48.54	-105.62550	40.36058
NDF24	3,321	157.99	63.37	-105.66524	40.40036
NDF25	2,922	163.30	52.20	-105.65147	40.31393
NDF26	2,623	80.54	45.62	-105.61381	40.33877
NDF27	2,605	129.47	55.06	-105.55036	40.21604
NDF28	2,705	95.91	36.44	-105.53609	40.31094
NDF29	2,647	196.26	62.50	-105.61879	40.40546
NDF30	2,909	189.78	73.57	-105.69110	40.42281
NDF31	2,816	152.93	74.35	-105.64110	40.31094
NDF32	2,836	111.51	44.34	-105.65110	40.39762
NDF33	2,763	187.31	72.74	-105.67040	40.41690
Mt Meeker	3,451	48.81	53.15	-105.58677	40.24669
N St Vrain	2,929	267.44	89.18	-105.57470	40.19614
Twin Sisters West	3,081	278.62	40.31	-105.52883	40.29345
Cow Creek	2,638	169.70	111.80	-105.52261	40.43317
Black Canyon N	2,903	204.53	126.42	-105.55416	40.41505
Black Canyon S	2,940	160.11	62.47	-105.57169	40.40985
Bighorn	2,747	189.16	78.50	-105.58893	40.40964
Little Debbie	3,040	258.69	44.62	-105.52847	40.28819
Lumpy Ridge	2,687	191.31	95.61	-105.54498	40.41072
Highway 7	2,836	84.04	84.21	-105.53919	40.31922
Pierson Park	3,180	82.48	66.83	-105.51105	40.28737

Name	Vegetation	Avg. soil depth (dm)	Max. soil depth (dm)	Deepest 3 soil depth (dm)	Percent Fines	Percent Organics
NDF1	brush	3.95	9	7	3.47	0.06
NDF2	brush	5.8	14	13	2.63	0.23
NDF4	brush	0.15	1	1.0	7.61	3.14
NDF5	coniferous	3.85	5	5.0	8.80	0.61
NDF6	coniferous	4.7	8	7.3	15.06	2.38
NDF7	coniferous	2	5	4.0	2.37	1.28
NDF8	coniferous	4.95	8	7.0	3.10	0.42
NDF9	brush	2.7	7	6.0	5.71	0.74
NDF10	brush	2.9	8	6.0	1.83	0.02
NDF11	coniferous	3.2	5	4.7	5.67	0.52
NDF12	herbaceous	5.1	10	8.3	11.85	0.17
NDF13	brush	6.45	10	9.7	3.42	0.04
NDF14	coniferous	6.4	10	9.7	2.28	0.42
NDF16	coniferous	3.1	6	5.3	6.99	0.11
NDF17	brush	3.1	6	5.0	3.84	0.01
NDF18	brush	5.7	12	10.7	8.09	0.02
NDF19	coniferous	5	10	8.0	8.56	1.19
NDF20	coniferous	4.3	8	7.3	3.86	0.73
NDF21	coniferous	5.5	8	7.7	2.97	0.09
NDF23	coniferous	4.9	9	8.0	4.62	2.01
NDF24	coniferous	2.6	5	4.7	10.75	3.48
NDF25	coniferous	4.3	7	6.3	4.29	0.13
NDF26	brush	2.9	5	4.3	8.51	0.05
NDF27	brush	3.7	7	6.3	8.70	0.09
NDF28	coniferous	4.3	7	6.7	6.32	0.45
NDF29	herbaceous	2.7	4	3.7	3.51	0.39
NDF30	coniferous	3.45	7	5.7	7.33	1.08
NDF31	coniferous	3.3	5	5.0	8.26	0.40
NDF32	coniferous	6.45	10	9.3	5.89	0.55
NDF33	coniferous	3.4	6	5.0	6.36	0.64
Mt Meeker	brush	5.2	14.0	10.0	5.64	2.53
N St Vrain	coniferous	4.1	9.0	7.7	4.00	0.27
Twin Sisters West	coniferous	4.9	9.0	8.0	7.77	0.82
Cow Creek	brush	10.7	15.0	14.7	1.49	0.19
Black Canyon N	coniferous	3.5	6.0	5.7	2.49	0.26
Black Canyon S	brush	2.6	6.0	5.0	10.24	0.19
Bighorn	coniferous	4.3	10.0	7.3	3.52	0.21
Little Debbie	alpine	1.2	5.0	4.0	3.49	0.68
Lumpy Ridge	coniferous	4.6	7.0	7.0	3.05	0.26
Highway 7	coniferous	1.9	5.0	4.3	4.01	0.14
Pierson Park	coniferous	3.7	10.0	7.0	13.53	0.23

Name	Colluvial Hollow	Convergent Topograph.	General Curvature	Planform Curvature	Contrib. Area (m^2)	Last Fire
NDF1	no	no	1	0.993	612	--
NDF2	yes	yes	2	1.702	236	--
NDF4	no	no	1	0.017	420	--
NDF5	no	no	-2	-1.473	236	1536
NDF6	no	no	2	0.746	3103	1860
NDF7	no	no	-2	-0.600	5187	--
NDF8	no	no	-4	-1.024	1442	--
NDF9	no	no	0	0.000	1308	--
NDF10	no	no	9	1.022	5567	--
NDF11	no	no	0	0.250	821	--
NDF12	no	no	0	0.905	1704	--
NDF13	no	no	1	1.041	2513	--
NDF14	no	no	-4	-1.996	236	1880
NDF16	no	no	1	1.000	630	1859
NDF17	no	no	-1	-0.047	839	--
NDF18	no	no	0	0.150	9503	--
NDF19	no	no	0	-0.096	521	--
NDF20	no	no	2	1.000	4127	--
NDF21	no	no	1	-1.032	1457	--
NDF23	no	no	-3	0.000	41828	--
NDF24	no	no	-1	-1.030	1325	1721
NDF25	no	no	1	0.917	423	--
NDF26	no	no	2	1.000	3683	--
NDF27	no	no	2	1.000	6092	--
NDF28	no	yes	-2	-0.790	1228	--
NDF29	no	no	1	-0.195	1536	--
NDF30	no	no	-2	-1.219	935	--
NDF31	no	no	-6	-1.956	10676	1893
NDF32	no	no	3	2.466	8112	1924
NDF33	no	no	-4	-0.640	5476	--
Mt Meeker	no	yes	-1	-0.071	45761	--
N St Vrain	no	yes	-8	-0.933	465141	1978
Twin Sisters West	yes	yes	-1	-1.046	11113	--
Cow Creek	no	no	0	0.000	1555	--
Black Canyon N	yes	yes	-2	-0.611	669	--
Black Canyon S	no	no	0	0.150	566	--
Bighorn	yes	yes	2	0.031	1436	--
Little Debbie	no	yes	-3	-2.271	31727	--
Lumpy Ridge	yes	yes	1	0.892	279	--
Highway 7	no	no	-1	-0.072	2624	--
Pierson Park	no	yes	5	0.040	22321	--